國立交通大學

物理研究所

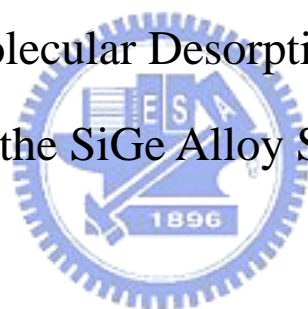## 碩士論文

氫分子在矽鍺合金表面熱脫附現象之研究

Hydrogen Molecular Desorption Mechanism

from the SiGe Alloy Surfaces

研 究 生：謝明峰

指導教授：林登松 教授

中華民國九十三年六月

氫分子在矽鍺合金表面熱脫附現象之研究

Hydrogen Molecular Desorption Mechanism

from the SiGe Alloy Surfaces

研 究 生：謝明峰　　　　　　　　Student：M.F. Hsieh

指導教授：林登松　　　　　　　　Advisor：D.S. Lin

國 立 交 通 大 學

物 理 研 究 所

碩 士 論 文

A Thesis

Submitted to Institute of Physics

College of Science

National Chiao Tung University

in partial Fulfillment of the Requirements

for the Degree of

Master

in

Physics

June 2004

Hsinchu, Taiwan, Republic of China

中華民國九十三年六月

氫分子在矽鍺合金表面熱脫附現象之研究

學生：謝明峰　　　　　　　　　　　　　指導教授：林登松 教授

國立交通大學物理研究所碩士班

摘　　要

本論文在研究氫分子在鍺/矽(100)表面的熱脫附現象，所使用的樣品為覆蓋率 0.4 ML 和 0.8 ML 鍺的矽(100)表面。實驗方法是利用掃瞄穿遂顯微鏡 (STM) 以及核心層光電子激發術 (core-level photoemission) 觀測氫脫附過後的樣品表面，以探討氫分子從表面上的 Ge-Ge、Ge-Si 以及 Si-Si 雙原子單體 (dimer) 結構而進行熱脫附的機制。氫分子熱脫附後，會在鍺矽表面留下懸結鍵對 (dangling bond pairs, DB pairs)，因此氫分子熱脫附的數量，即是在 STM 觀測影像上所直接計數的懸結鍵對數目。而在核心層光電子激發術的實驗中，我們將氯原子連結到氫熱脫附後的懸結鍵上。然後由 Cl $2p$ 的核心層光電子能譜的 Cl-Ge 分量與 Cl-Si 分量，可推得懸結鍵在鍺或矽原子上的分佈情形。結合掃瞄 STM 與核心層光電子激發術這兩種互補的顯微與光電子能譜技術，可以對氫分子熱脫附的機制進行更詳細的分析。

Ge-H 鍵的鍵結能比 Si-H 鍵要弱。在理想狀態下，在較低的加熱溫時氫分子應從 Ge-Ge 雙原子單體開始脫附，在稍高的溫度由 Ge-Si 脫附，在更高的溫度才會由 Si-Si 脫附。假設氫分子只是單純的由鍺/矽(100)表面的雙原子單體結構進行熱脫附，那麼在較低的溫度時，氫分子大部分是由 Ge-Ge 與 Ge-Si 雙原子單體上脫附。因此在 Cl $2p$ 核心層光譜中，Cl-Ge 分量應大於 Cl-Si 分量。但是在實驗結果的分析，卻是 Cl-Si 分量大於 Cl-Ge 分量。而最近有文獻指出，氫分子在熱脫附的過程中表面的鍺矽原子可能會互相交換，使得大部分的 Ge-Ge 雙原子單體轉換成 Ge-Si 雙原

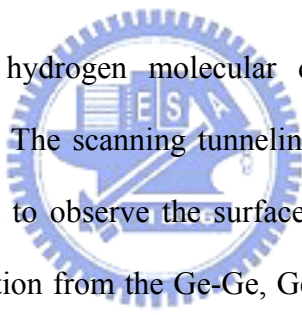子單體。根據這個論點來進行分析，所推得的結果與我們的實驗大致符合，因此我們判斷在氫分子熱脫附的過程中，表面的鍺原子的確會與矽原子進行交換。

Hydrogen Molecular Desorption Mechanism

from the SiGe Alloy Surfaces

Student: Ming-Feng Hsieh   **Adviser: Dr. Deng-Sung Lin**

Institute of Physics
National Chiao Tung University

ABSTRACT

We have studied the hydrogen molecular desorption from the 0.4-ML- and 0.8-ML-Ge/Si(100) surfaces. The scanning tunneling microscopy (STM) and core-level photoemission are employed to observe the surfaces after H_2 desorption and study the mechanism of the H_2 desorption from the Ge-Ge, Ge-Si, and Si-Si dimers. The dangling bond (DB) pairs will reappear on the Ge/Si surface after H_2 desorption, so the number of DB pairs in the STM images equals the coverage of H_2 desorbed from the surface. In the core-level-photoemission experiment, we terminated the DB pairs by the chlorine atoms before taking spectra. The analysis of the Cl-Ge and Cl-Si components in the Cl $2p$ core-level spectra could figure out the DBs upon Ge atoms and Si atoms. Combining these two powerful microscopic and spectroscopic techniques, the detailed information about the mechanism of H_2 desorption can be obtained.

The energy of a Ge-H bond is lower than that of a Si-H bond. Therefore in ideal case, the hydrogen molecules will start to desorb from Ge-Ge dimers at a lower temperature, from Ge-Si dimers at a middle-high temperature, and from Si-Si dimers at a high

temperature. Assuming that hydrogen molecules simply desorb from the dimer structure, the most hydrogen molecules will desorb from the Ge-Ge and Ge-Si dimers at lower temperature. Consequently, the intensity of the Cl-Ge component will be larger than that of the Cl-Si component in Cl $2p$ core-level spectra. However, the experimental result indicated that the intensity of the Cl-Si component was larger than that of the Cl-Ge component. The recent reports suggested that the exchange of Ge and Si atoms will occur during the H_2 desorption from Ge/Si surface making the most Ge-Ge dimers transform into the Ge-Si dimers. According to this argument, the result is roughly in agreement with our experiment. Therefore, the replacement of Ge/Si atoms likely occurs during H_2 desorbing from the Ge/Si(100) surface.

TABLE OF CONTENTS

CHAPTER 1

INTRODUCTION

1.1   Motivation

The band gap of Germanium (0.67 eV) is lower than which of Silicon (1.12eV) thus making heterostructure of the SiGe alloy has practical applications to optical and electronic devices [1-2]. In modern applications, the heterostructure of the SiGe has been used in 90-nm complementary metal-oxide-conductor, SiGe heterojunction bipolar transistor bipolar transistor, radio frequency Integrated circuit, Bluetooth, cell phone, multi-junction solar cells, and etc. Therefore, the correlative studies of the Ge_xSi_{1-x} alloy are very important to semiconductor industry.

Growth of Ge_xSi_{1-x} often uses gas-source molecular beam epitaxy (MBE) and chemical vapor deposition (CVD) technique [3-5]. Hydrogen desorption is an important process controlling the growth rate of Ge_xSi_{1-x} in CVD and has been studied by various groups [6-9]. Resent reports demonstrated that Ge and Si atoms in the surface layers would exchange their places during H_2 exposure on the surface of GeSi alloy [10-12]. Although the H_2 desorption from the Ge/Si(100) surfaces has received extensive attention, several fundament questions regarding the mechanism of H_2 desorption from three types of dimers (Ge-Ge, Ge-Si, and Si-Si) and the place exchange of the Ge/Si atoms during the desorption remain unclear. The purpose of our study was to improve the understanding of the mechanism of the H_2 thermal desorption from the heterostructure of the GeSi alloy.

1.2 The Clean Si(100)-2x1 Surface

Because the Si(100)-2x1 surface is the substrate on which we grow Ge films, its atomic structure of surface will be introduced first as following. Silicon is a group IV element with four electrons in its outer orbit. In a silicon crystal, each silicon atom has four valance bonds bonded to four neighboring silicon atoms in tetrahedral form. The crystal structure of Si is diamond structure with a lattice constant of 5.43 Å, as shown in Fig. 1.1.

(a)   (b)
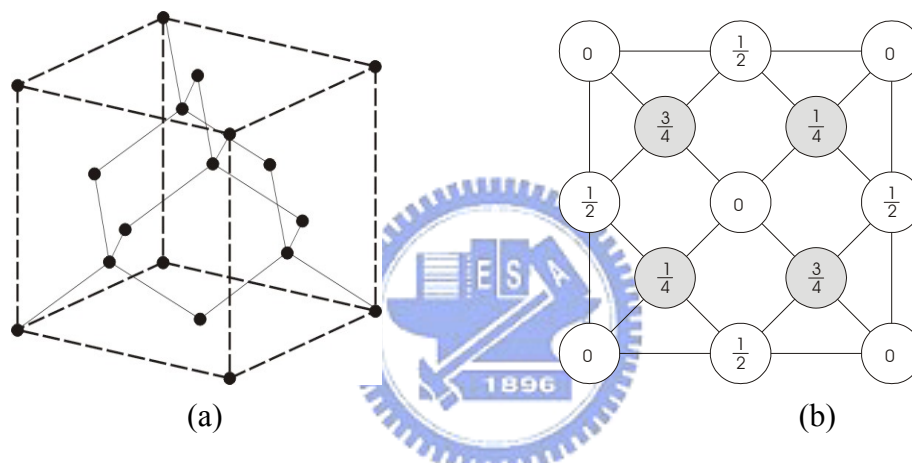
Fig. 1.1. (a) Diamond structure, showing the tetrahedral bond arrangement. (b) The down view of diamond structure, the fractions denoted the height of the atoms in units of a cubic edge.

When the Si crystal is cleaved along a different crystal orientation, the new surface will reconstruct into different surface atomic structure. For example, if the crystal is cleaved along the (100) direction, the exposure surfaces will reconstruct into 2x1 structure. If the crystal is cleaved along the direction normal (111) direction, the new surface will reconstruct into 7x7 structure. In this section, we will discuss the detail of the Si(100)-2x1 structure.

If one cleaves the silicon crystal along the (100) direction, two valence bonds of each Si atom at the exposed surface will be broken and transform into dangling bonds. Therefore, every silicon atom in the surface has two dangling bonds and two valence bonds, as shown in Fig. 1.2.
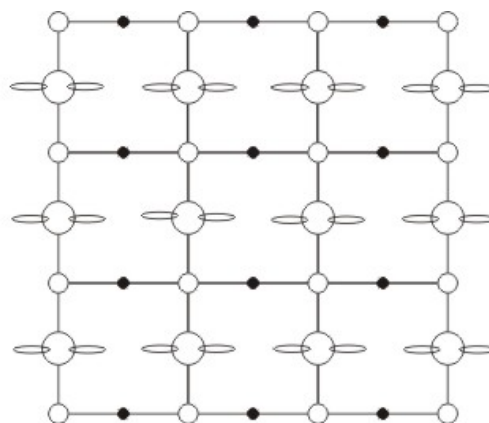

Fig. 1.2. The side view of the ideal Si(100) surface. Each silicon atom has two valence bonds and two dangling bonds.

Figure 1.3 displays the top view of this unreconstructed Si(100) surface with 1x1 structure. In this 1x1 structure, the density of the dangling bonds is high (two dangling bonds per atoms), therefore the surface energy is high and the 1x1 structure is unstable. To reduce the numbers of the dangling bonds, the first layer atoms in the surface will reconstruct. By this way, the surface energy will be lower and the 1x1 structure will be more stable.

Upon reconstruction, two neighboring atoms form a strong sigma (σ) bond by combined one of the two dangling bonds. The amount of dangling bonds is reduced by 50%. These remaining dangling bonds can further form a weak pi (π) bond, as shown in Fig. 1.4. The 1x1 structure of the surface have transformed into 2x1 structure, as shown in Fig. 1.5. These bonded pairs of Si atoms are called dimers.

(a) top view
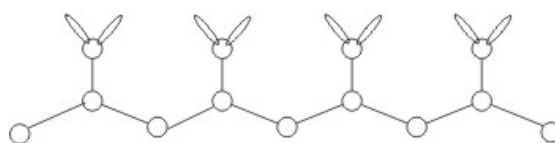
(b) side view

Fig. 1.3. (a) The top view of the ideal Si(100)-1x1 surface. ◯ : the first layer atoms; ◯ : the second layer atoms; ● : the third layer atoms. (b) The top view of the ideal Si(100)-1x1.
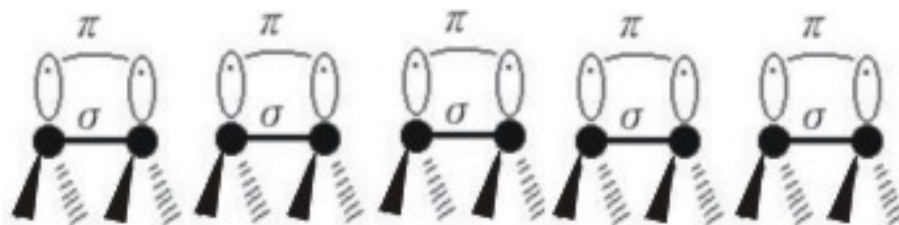
Fig. 1.4. The side view of the Si (100)-2x1 first layer surface structure.
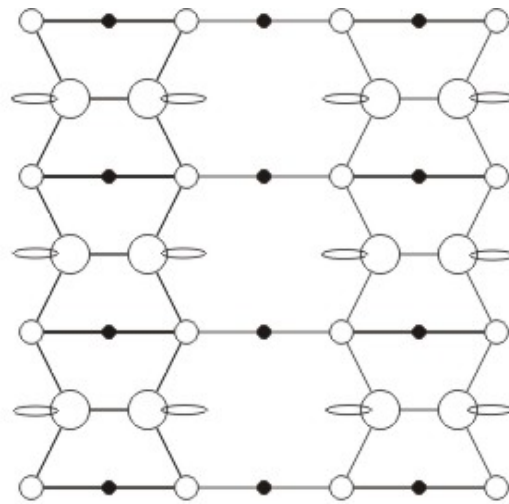
(a) top view
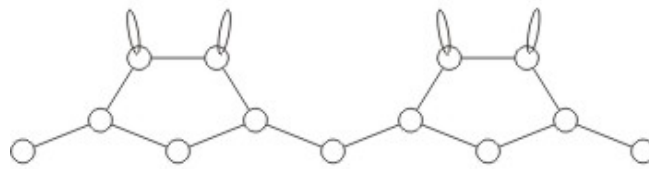
(b) side view

Fig. 1.5. Top view (a) and side view (b) of the Si(100)-2x1 structure . ◯: the first layer atoms. ◯: the second layer atoms. ●: the third layer atoms.

When preparing the Si(100) surface, the step structure formed by the cleavage along the (100) direction, as shown in Fig. 1.6. The height of the step is about 1.36Å. The dimer rows on the neighboring terraces are perpendicular, so steps of the terraces divide into two types. S_A is the steps where the dimer rows direction on the upper terrace parallel the step edge. S_B is the steps where the dimer rows direction on the upper terrace perpendicular the step edge.
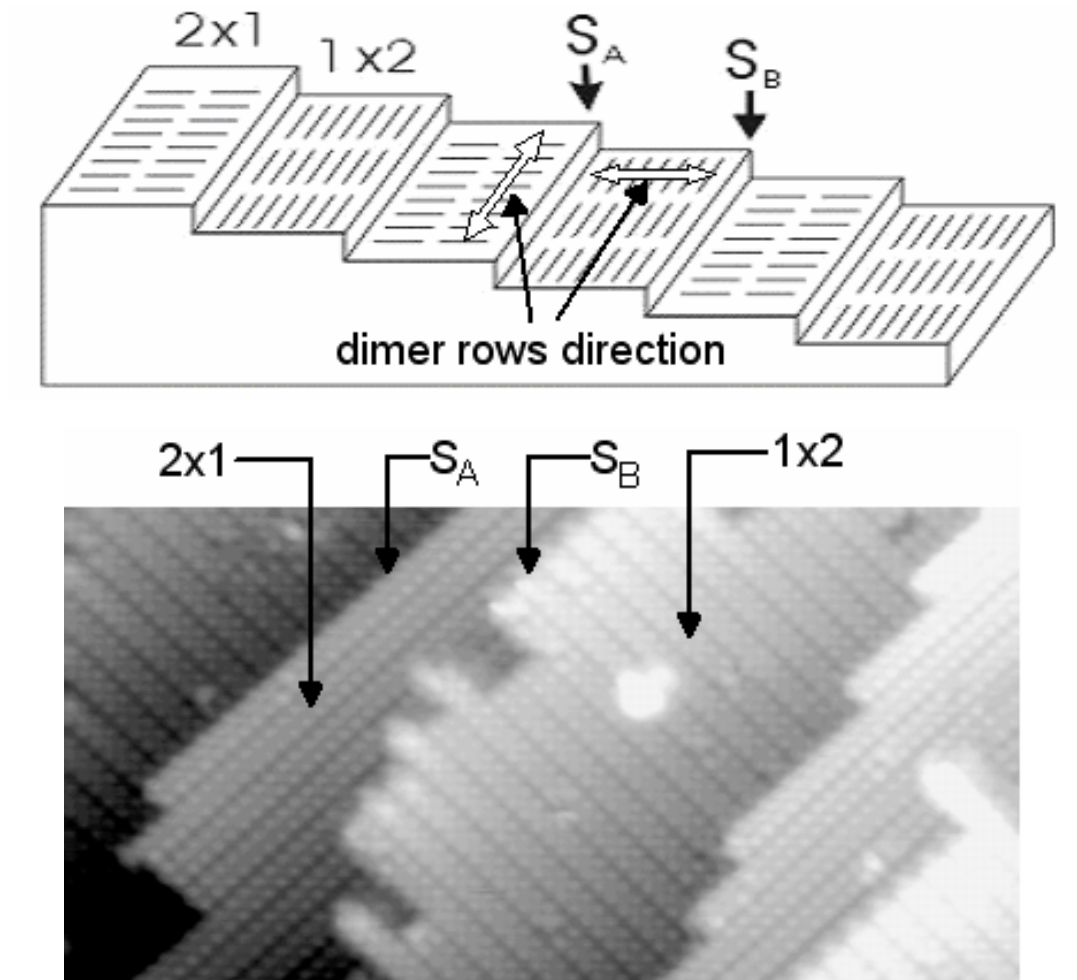
Fig. 1.6. Step structure, S_A and S_B, on the Si(100)-2x1 surface. S_A is the steps where the dimer rows direction on the upper terrace parallel the step edge. S_B is the steps where the dimer rows direction on the upper terrace perpendicular the step edge. The bottom picture shows STM image which size is 200x100 Å^2 and the sample bias is +2 V.

1.3   The Ge/Si(100) Surface

In this section, we mainly intend to introduce the atomic-layer epitaxy (ALE) and the resultant surface investigated by scanning tunneling microscopy (STM). By our previous works [6], exposure of 15 L (langmuir, 1 L=10^{-6} torrs-sec) digermane (Ge$_2$H$_6$) onto the Si surface followed by annealing the substrate at 900 K for 60 seconds yields a net deposition of 0.4 ML Ge. Repeating the cycle growth results in a quantized deposition of Ge known as the atomic-layer epitaxy and forms a smooth film growth as indicated above. With the atomic-layer epitaxy, we can precisely control the deposition of Ge on the surface and observe the thermal reactions occurred on the low-dosage Ge/Si surface. We obtained the Ge/Si(100) sufaces of the various coverage by the cycle growth of Ge on the Si(100)-2x1 surface at RT.

In order to obtain a detailed investigation of the spatial distribution of Ge atoms deposited on Si(100) by ALE, the chlorine atoms are terminated on the mixed Ge/Si(100) surface to enhance the contrast between Ge and Si sites in STM observations [6]. Furthermore, there is an unusually large chemical shift between Cl adsorbed on Si and Ge atoms, and this result can aid the core-level photoemission measurements [6, 16-17]. The detail information will be presented in the latter sections. The STM and core-level photoemission spectroscopy techniques form a power combination of surface analysis and the method chosen for this present study.

7

1.4 Literature Review

1.4.1 H_2 Desorption Mechanism from the Monohydride Structure

Because hydrogen induces three reconstructions 1x1, 2x1, and 3x1 on the H-saturated Si(100) surface at different substrate temperature, the H_2 desorption from monohydride and dihydride structure becomes more complex. In order to simplify the desorption problem, the monohydride reconstruction, 2x1 dimer form, was prepared for our study. The previous studies indicate that the desorption mechanism of monohydride on Si(100)-2x1 [18] and Ge(100)-2x1 [19] consist of a pairing model, in which a paired set of hydrogen atoms desorbs from a single dimer unit, as shown in Fig. 1.8. Therefore, we deduce that the same H_2 desorption mechanism occur on the Ge/Si(100)-2x1 surface.
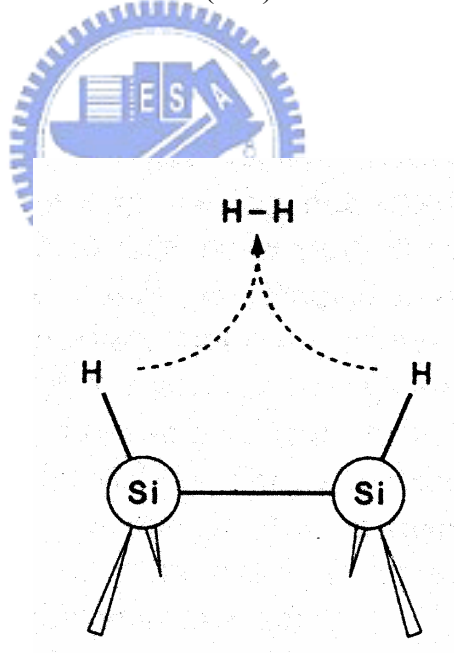

Fig. 1.8. The H_2 desorption mechanism of monohydride on Si(100)-2x1 consist of a pairing model, in which a paired set of hydrogen atoms desorbs from a single dimer unit.

1.4.2   The H-saturated Si(100) Surfaces

Chemical vapor desorption (CVD) of hydrogen on the surface of semiconductors has received much attention because hydrogen can readily react with the surface dangling bonds and forms stable hydrides. In addition, hydrogen is one of the simplest adsorbates to study adsorption, reaction, and desorption processes on the semiconductors and serve as prototype. Therefore, we must understand the H-saturated Si(100) surfaces first. Atomic hydrogen causes a strong interaction with surface states and becomes a powerful tool to assist us with identifying different surface states. Hydrogen is known to induce the reconstructions, 1x1, 2x1, and 3x1 structures, on the Si(100) surfaces as shown in Fig. 1.7 [13-15].

Boland *et al.* indicated that, a monohydride phase would form a dimer structure on the surface when exposing H atoms on the Si(100)-2x1 surface on a typical condition at RT [13]. After further adsorption of hydrogen at RT, the dimer bonds break and form the dihydride phase. The dihydride phase finally reconstructs the 1x1 structure. When exposing H on the Si(100) surface at about 370 K, the monohydride and dihydride phases compose the 3x1 structure. The dihydride and monohidride phases can be easily identified by STM as reported by Boland *et al.* When we expose H on the Si(100) surface at about 650 K, the surface exhibits a 2x1 dimer structure. The hydrogen-adsorption temperature in our work is about 600 K, in other words, the surface should mainly exhibit a monohydride phase as introduced.

Figure 1.7 shows a model for the three reconstructions 1x1, 2x1, and 3x1 structures on the H-saturated Si(100) surfaces [13-14]. Irradiation of atomic H beam on the initially monohydride surface leads to the formation of dihydrides and repulsive stress between them.   At T_S < 310 K, inhomogenious 1x1 structure is formed, and reconfiguration to

dimers with moleuclar hydrogen emission does not proceed. At 360 K < T_S < 480 K, the surface has 3x1 structure with mono-hydride and dihydride next to each other, and the desorption of hydrogen molecules is less efficient. At T_S > 480 K, reconfiguration to monohydride dimers proceed via emitting hydrogen molecules. The STM images are obtained from J. J. Boland, 1990 [13].
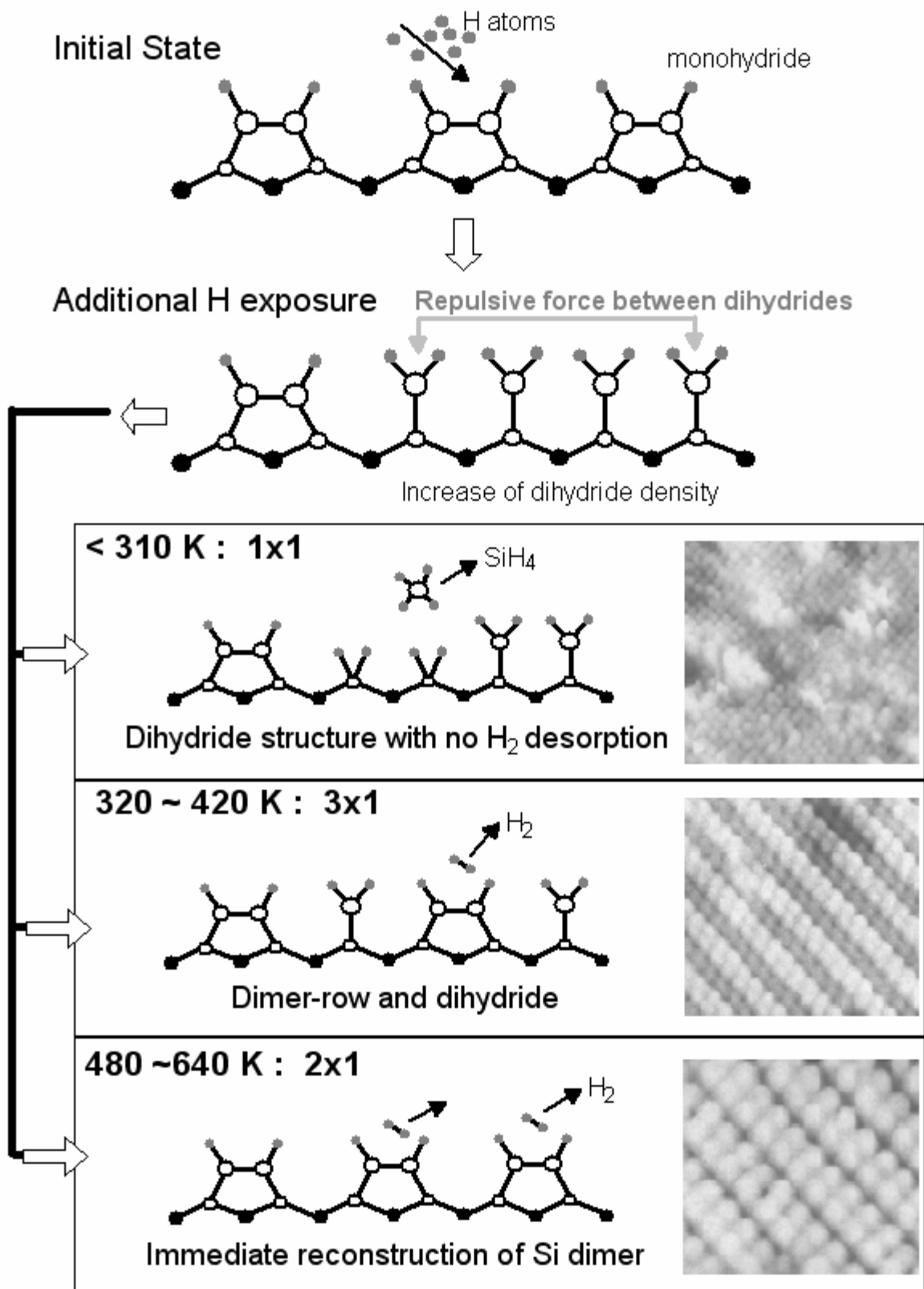
Fig. 1.7. Model for the 1x1, 2x1, and 3x1 reconstructions on the H-saturated Si(100) surfaces [14] . The STM images are obtained from J. J. Boland, 1990 [13].

1.4.3　Place Exchange of Ge and Si Atoms

Among the previous works of the exchange reaction of the Si and the Ge atoms induced by hydrogen, Rudkevich *et al.* offered definite evidences with the Si(100)-2x1 surface deposited with about 1.3-ML Ge [10]. In Ref. [10], the authors prepared the about 1.3-ML Ge/Si surface by CVD and the coverage was determined from RHEED observations. The Ge/Si surface was investigated by Fourier transform infrared- attenuated total reflectance (FTIR-ATR) spectroscopy. After growth of the Ge, atomic hydrogen saturated the sample surface by using resistively heated tungsten filament to dissociate molecular H_2. The corresponding FTIR spectrum shows two strong peaks at 1980 and 2000 cm^{-1} originated from Ge-H stretching mode.

After obtaining the base spectrum for the prepared surface, the authors raised the temperature to 330 ℃ and repeatedly dosed with hydrogen to ensure saturation of the dangling bonds. The resultant spectrum shows a increasing of the Si-H peak and a decreasing of the Ge-H peaks obviously. To ensure this process reversible, the authors annealed the H-covered surface at 550 ℃ to dispel the hydrogen completely, and re-dosed the Ge/Si surface with hydrogen at RT. The corresponding spectrum shows strong Ge-H peaks and nearly invisible Si-H peaks as originally shown in the base spectrum.　From the series of the spectra, the exchange reaction between Si and Ge near the surface layer is evident.

To explain the mechanism of the replacement reaction, the authors proposed an atomic model. For observing a low temperature extent of the exchange reaction (about 250 ℃), the low temperature extent was associated with a kinetic process of lower barrier than breaking Si-Ge bonds. The authors therefore postulated that the exchange reaction does not occur except in the region that defects can lower the barrier, as shown in Fig.1.9. They proposed

that, on the clean Si(100) surface, dimers can exchange place with two subsurface atoms through the migration of a dimer vacancy in a concerted motion of several atoms without bonds breaking. The model of the exchange reaction between Ge and Si atoms was built up in the similar way, except replacing Si dimers by H-terminated Ge dimers. Migration of the dimer vacancy results from the addition of hydrogen can lead to the direction that the replacement reaction occurred as observed.
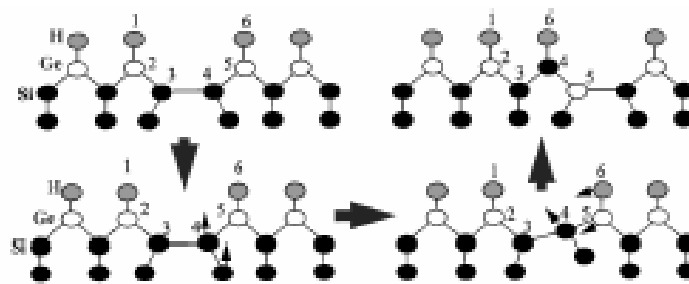

Fig. 1.9 Models of the proposed place exchange mechanism and structure. The Ge/Si place exchange reaction occurs at the dimer vacancy [10].

Angot *et al.* confirmed this Ge/Si exchange and further suggested that H may energetically favor the mixed Ge-Si dimers than the pure Ge-Ge dimers during H exposure on the Ge/Si(100) surface at high temperature (above 200 ℃) [11].

CHAPTER 2

EXPERIMENTAL DETAILS

2.1 The Vacuum System

The STM experiment was conducted in an ultrahigh-vacuum (UHV) system. The main chamber is equipped with a VT-STM (Omicron), a manipulator, a pumping system, gas sources including H2, Cl2 and G2H6, as shown in Fig. 2.1. The pumping system is consisting of a dry pump, a turbo pump, a titanium sublimation pump (TSP) and an ion pump. The base pressure of this vacuum system is 2×10^{-10} torr.

We use a dry pump to lower pressure in the vacuum chamber to $\sim 10^{-3}$ torr. The turbo pump automatically starts to lower the pressure to the 10^{-6} torr range. At this lower pressure, the ion pump turns on. As the pressure drops to $\sim 10^{-7}$, we start to bake the chamber at about 120 ℃ for over 24 hours. After the chamber cools down to RT, we gain the ultra-high vacuum about 2×10^{-10} torr.

The core-level-photoemission experiment is carried out at the Synchrotron Radiation Research Center located in the Hsin-chu Science-based Industrial Park, Taiwan. Light from the 1.5-GeV storage ring was dispersed by a Dragon-type 6-m wide range spherical grating monochromator (SGM). This beamline has two energy range, *i.e.* 10-175 eV from a low energy branch and 120-1500 eV from a high energy branch. In our experiment, we use the high energy branch since the main photon energy used are 135, 140, and 240 eV. All the Ge_2H_6 adsorption, annealing, and Ge film growth were prepared *in situ* in the ultra-high vacuum system. In the photoemission experiment, the procedure to obtain the ultra-high vacuum is the same as the STM experiment.
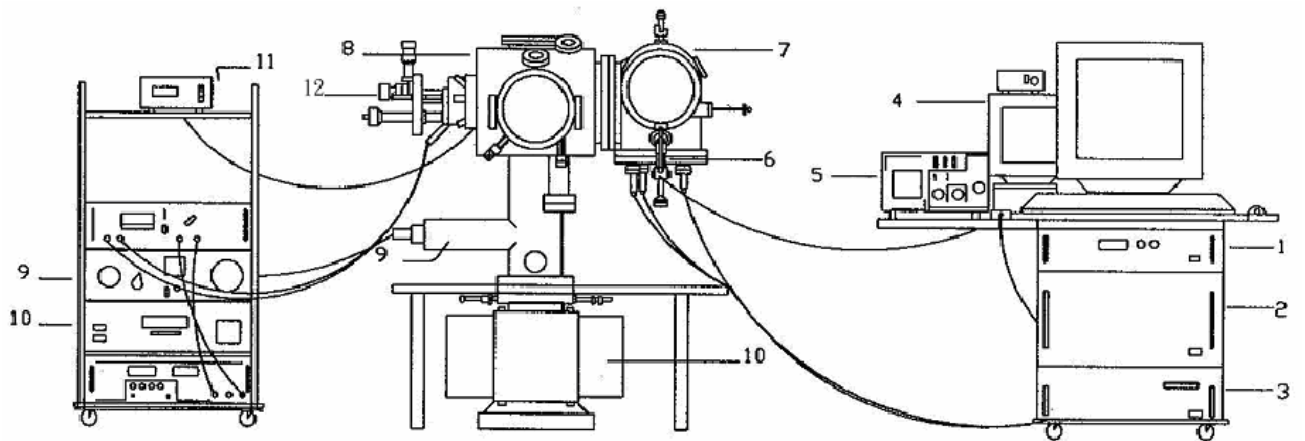
Fig. 2.1 The side view of the whole STM system. 1. STM variable temperature controller; 2. STM hardware controller; 3. STM work station; 4. CCD camera monitor; 5. Oscilloscope; 6. CCD camera; 7. STM chamber; 8. Main chamber; 9. TSP and TSP controller; 10. Ion pump and ion pump controller; 11. Ion gauge; 12. Manipulator (adapted from Perng-Horng Wu, 1997).

Fig. 2.2. The side view of the core-level-photoemission vacuum system. It contains two vacuum chambers, a combination of pumps, a hemispherical analyzer, a manipulator, and a computer. The pump combination includes a mechanical pump, a turbo pump, two ion pumps, and a titanium sublimation pump (TSP).

15

2.2 Scanning Tunneling Microscopy (STM)

Since Binnig *et al.* invented the Scanning Tunneling Microscopy (STM) and obtain the atomic resolution in 1982, the STM technique has been widely used in various fields, like condensed-matter physics, chemical, biology physics and etc.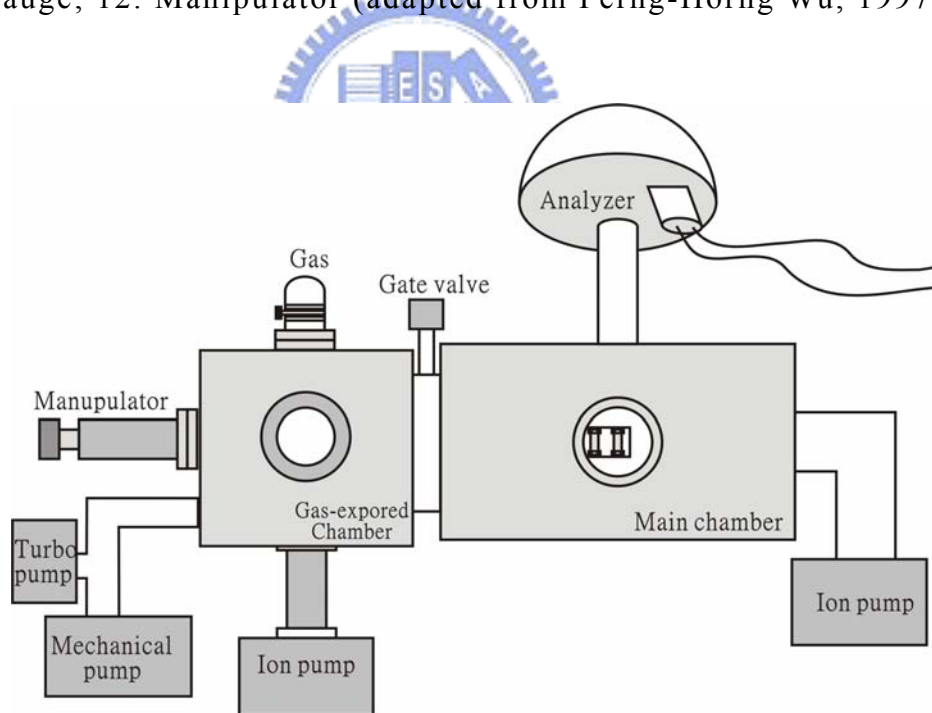 Especially, after resolving the structure of the Si(111)-7x7 in real space using STM , this instrument has proved to be an extremely powerful tool.
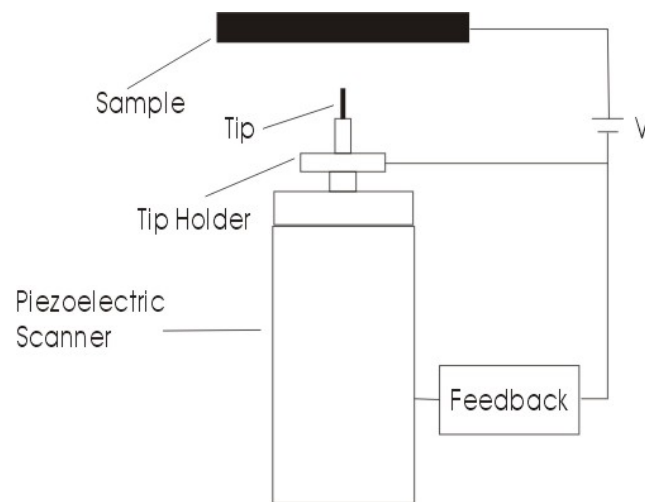
Fig. 2.3. Schematic diagram displays the essential elements of STM.

Figure 2.3. displays its essential elements. A probe tip, usually made of tungsten (W) or Pt-Ir alloy, is attached to a piezoelectric scanner. Using the coarse positioner and the z piezo, the tip and the sample are brought to within a few angstroms of each other. A bias voltage, applied between the tip and the sample, causes an electrical current to flow. This is a quantum-mechanical phenomenon, tunneling, which is the principle theory of the scanning tunneling microscopy. To achieve atomic resolution, vibration isolation is essential. A commonly used vibration isolation system consists of a set of suspension springs and a damping mechanism.

The operating principle of the STM is based on the quantum mechanical phenomenon of tunneling. In this section, we discuss the concept of the tunneling through one-dimensional model. First we consider the classical situation. In the classical mechanics, an electron with energy E moving in a potential U(z) is described by

$$\frac{p_z^{\ 2}}{2m} + U(z) = E,$$ (2.1)

In the regions where E > U(z), the electron has a nonzero momentum pz. It means that the electron has the ability to be in those regions. Otherwise, in the regions where E < U(z), the electron can not penetrate into those regions. In other words, the electron with energy E has no possibility to be find in the regions with U(z) >E. Now we discuss the quantum effect. In the quantum mechanics, the motion of the same electron is described by the Schrödinger's equation,

$$-\frac{\hbar^2}{2m}\frac{d^2}{dz^2}\Psi(z) + U(z)\Psi(z) = E\Psi(z)$$ (2.2)
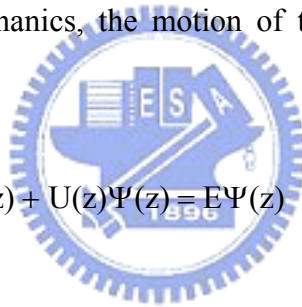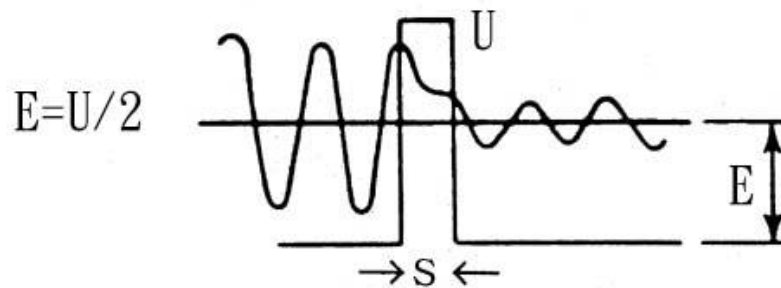
$\Psi(z)$ is the wavefunction of the electron.

Fig. 2.4. Wave function $\Psi(z)$ for an election with kinetic energy E = U/2 penetrating a potential barrier U.

For a electron with E = U/2 incident on a square barrier from the left, as shown in Fig. 2.3. The Schrödinger's equation of this electron

$$-\frac{\hbar^2}{2m}\frac{d^2}{dz^2}\Psi(z)+\frac{1}{2}U\Psi(z)=0$$

(2.3)

has the solution

$$\Psi(z)=\begin{array}{l}Ae^{ikz}+Be^{-ikz}..........(z<0),\\ Ce^{Kz}+De^{-Kz}............(0<z<s),\\ Fe^{ikz}.........................(z>s),\end{array}$$

(2.4)

where $k=\frac{(2mU)^{\frac{1}{2}}}{\hbar}$; $K=\frac{(mU)^{\frac{1}{2}}}{\hbar}$.

Eq. 2.4. can be solved for the transmission coefficient T = |F/A|2 by matching of the boundary conditions on Ψ and dΨ/dz at x = 0 and x = s. That is

$$T=\frac{1}{1+(\frac{k^2+K^2}{2Kk})^2\sinh^2 Ks}$$

(2.5)

Because a barrier of width s that is much thicker than the wave function decay length of 1/K, $Ks\gg 1$, the transmission coefficient can be approximated as

$$T\approx\frac{16k^2K^2}{(k^2+K^2)}e^{-2ks}$$

.

(2.6)

It is this exponential dependence of the transmission coefficient T on the barrier width s that enables atomic resolution images in tunneling microscopy. It provides a sufficient signal, the tunneling current, for atomic scale feedback control of the gap width s along the z direction.

2.3   Core Level Photoemission

The core level photoemission experiment is to collect the photoelectrons excited from core level near nucleus. Photoelectrons were collected and analyzed by a large hemispherical analyzer. By measuring the variation of the photoelectron kinetic energy, we can observe the species of the passivated atoms and chemical bonding etc.

The photoelectrons are excited from inner energy levels (binding energy >20 eV), of which the orbital radius is less than 0.3 Å. In solid state, the core level wave functions are independent such that the binding energies of the atoms in bulk are the same. However, the potential of the atoms near surface becomes different because the local atomic environment changes. The potential difference of surface atoms results in chemical shift of the core level binding energy.

We can explain the relationship between the kinetic energy (KE) of excited photoelectrons and energy of incident photons by the energy conservation law as Eq. 2.7. The relation of the energies is shown in Fig. 2.5.

$$KE = h\nu - B - \Phi \qquad (2.7)$$

KE : kinetic energy of excited photoelectron

hv: photon energy

B: binding energy
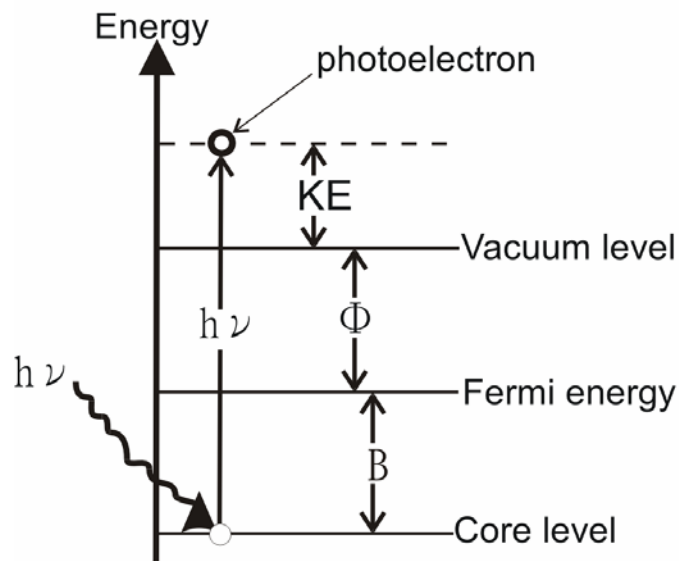
Φ: work function.

Fig. 2.5. Schematic for the energy levels in the core-level photoemission.

In this formula, the binding energy B is the difference between the core level and Fermi level. The work function Φ is the difference between the Fermi level and vacuum level. This formula is based on the ideal situations; however, we have to consider other factors like secondary electrons and escape depth etc. The escape depth of the excited photoelectron is dependent on the kinetic energy, in other word, the higher kinetic energy, the larger escape depth. Therefore, the escape depth of photoelectrons of kinetic energy 20 eV ~ 110 eV is less than 10 Å. The spectra obtained by analyzing these photoelectrons provide us the message of the surface.

After electrons excited from core level, left holes will be occupied by other electrons. The reaction of occupation can occur in two processes. First, the electrons in the higher energy level occupy the left holes and release the photons of energy equivalent to the difference between two levels. Next, the electrons in the higher energy level occupy the electron holes and release energy. The released energy is not carried by photons but directly

excites electrons to leave surface. The excited electrons in the second process are so-called Auger electrons. The Si 2p and Ge 3d core level photoemission is mainly contributed from Auger electrons.

The lifetime of the electron holes yields Lorentzian broadening. The other factor to result in broadening spectra is the resolution of the analyzer, which produces a Gaussian width of the spectra. The convolution of the Lorentzian width and Gaussian width yields a Voigt lineshape for the spectra.

2.4 Sample Preparation and Temperature Measurement

The Si(100) samples, of size 12 x 4 mm^2, were sliced from commercial p-type wafers with a resistivity of about 10 Ωcm. The misalignment of the wafer is about 0.1 degree. Before tranfering the sample into the vacuum chamber, we blow dusts off the surface of the sample with pure nitrogen gas. In the UHV chamber, the sample is degased over 16 hours at ~800 K using a small AC current (300 mA). After degassing, the sample was flashed at ~1400 K for 8 seconds twice (cool down the sample, then repeat the flash process again) in order to remove the oxide layer on the surface and form a clean Si(100)-2x1 surface.

After flashing, the Si(100)-2x1 surface was exposed over 30-L (1×10^{-6} torr for 30 sec) gaseous digermane (Ge_2H_6) at RT.   Then the sample was annealed at 950 K to desorb the hydrogen and leave behind a net deposition of 0.4-ML Ge on the Si(100)-2x1 surface.   By repeating the Ge_2H_6 exposure and annealing one more time, we can gain the 0.8-ML Ge depositing on the Si(100)-2x1 surface [5].

After the growth of Ge/Si(100)-2x1, a spiral tungsten filament, which was placed approximately 5 cm from the sample was heated at 1800 K. The hydrogen gas was introduced into the chamber at 1×10^{-7} torr for 12 min (72 L) to saturate the sample surface. Finally, we procee to desorb the hydrogen molecules on the Ge/Si(100) surface at various temperatures for 1 min and then expose the chlorine gas for 30 sec at a backgroune pressure of 1×10^{-8} torr to terminate the dangling bonds.

Temperature of the sample can be controlled by the annealing current applied on the sample. In the experiments, measurement of the sample temperature is performed by two kinds of infrared pyrometers: one for the range from 250 to 650 ℃ and the other for the range from 600 to 1600 ℃. Because the pyrometer of the high-temperature range has better accuracy, we calibrate the other pyrometer with a 60-K offset and show the result in Fig. 2.6.
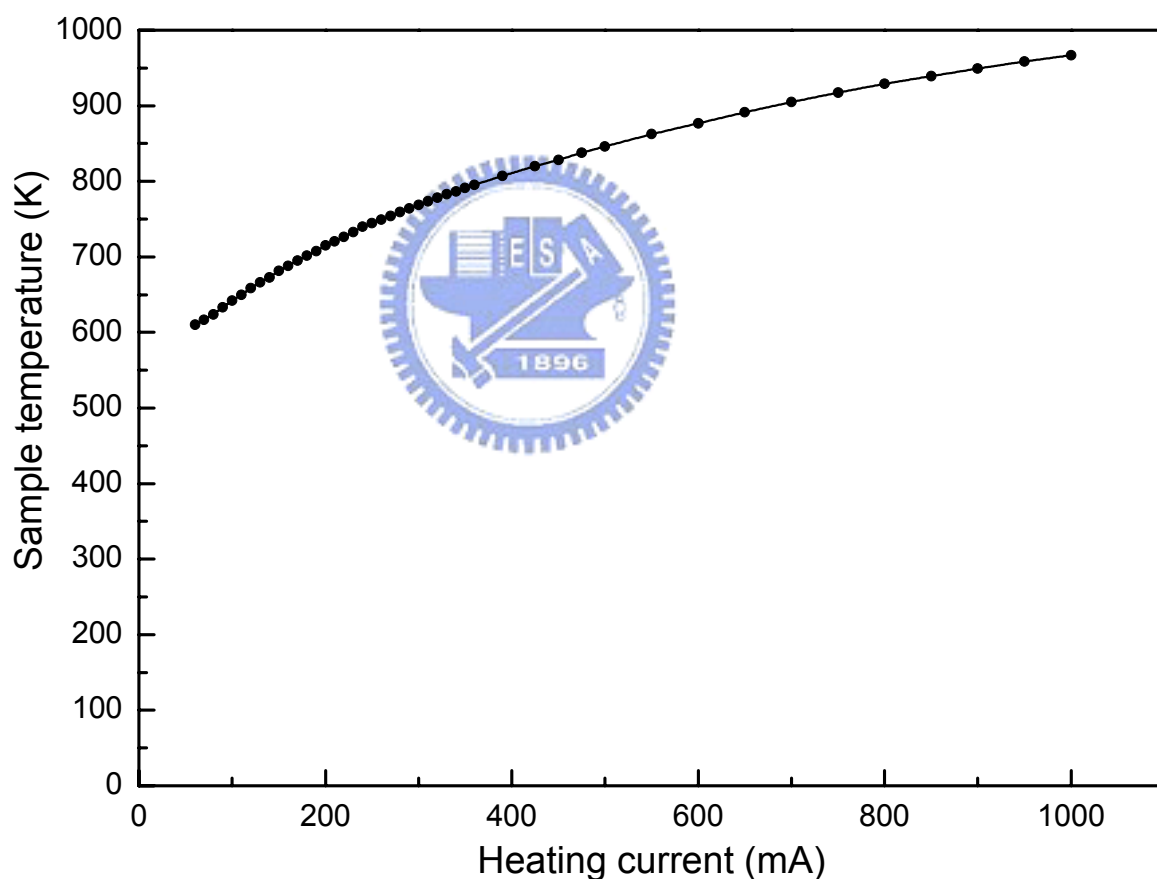

Fig. 2.6. A chart displays the sample current applied on the sample vs. its corresponding temperature.

CHAPTER 3

RESULTS AND DISCUSSIONS

Heterostructure of Ge/Si(100) has been extensively applied to photoelectric devices, and thermal chemical vapor deposition (CVD) technique is usually used to grow thin epitaxial alloy for these high-speed and high-gain devices. Digermane (Ge_2H_6) is the common chemical for CVD to form the GeSi alloy. However, the H_2 desorption is one of the process growing the GeSi heterostructure and also the simplest chemical desorption from the GeSi alloy. Therefore, the mechanism of the H_2 desorption is very important to the semiconductor industry. In this chapter, we will show both STM and core-level photoemission experiment data for H_2 desorption from the Ge/Si(100) surface.

The STM data gave the real-space images directly, so we could observe that DB pairs, remained after the H_2 desorption from dimer structure. Although the STM images showed desorption results obviously, it did not have sufficient information to identify the dimer types from which hydrogen molecules were desorbed. We could only obtain the amount of H_2 desorption from the Ge/Si surface.

Next, we exposed chlorine to terminate the DB pairs at the 0.4-ML and 0.8-ML Ge/Si(100):H surface after H_2 desorption. Because Cl-Si and Cl-Ge bonds had well-resolved energy shifts in Si $2p$, Ge $3d$ and Cl $2p$ core level spectra, we probably should analysis the compositions of dimers from which hydrogen molecules were desorbed. According to the comparison between STM and photoemission data, we could confirm the procedure of H_2 thermal desorption from the Ge/Si(100) alloy surface.

3.1 STM Observation and Analysis

Section 3.1 performed the STM data for the H_2 desorption on the 0.4-ML Ge/Si(100): 2x1 surface at the substrate temperature between 300 K and 784 K. The bright sites in the STM images represented the DB pairs which were formed by H_2 decomposing from the surface. The amount of DB pairs was proportion to the coverage of H_2 desorption. Therefore the counting of the bright sites indicated the coverage of H_2 desorption directly.

3.1.1 STM Images for the 0.4-ML-Ge/Si(100) Surface

Figure 3.1 (a) displays the STM image of the 0.4-ML Ge/Si(100) surface which was exposed to H_2 for 72 L ($1x10^{-7}$ torr, 12 min) at substrate temperature 600 K. The H-saturated 0.4-ML-Ge/Si(100) surface, as shown in Fig. 3.1 (a), maintained the 2x1 dimer structure which was the same as H-terminated Si(100)-2x1 surface. The big bright cluster site, black arrow in Fig. 3.1 (a), indicates SiC structure which was usually produced after annealing process. The little bright site, white arrow in Fig. 3.1 (a), indicates a DB pair remained on the surface. Because it was hard to deposit H atoms on the entire Ge/Si(100) surface, a few of DB pairs (lower than 2% of the entire surface area) would remain.

Fig. 3.1 (b)-(f) displayed the STM images after 1-min annealing process on the 0.4-ML-Ge/Si(100)-2x1:H surface at substrate temperature 592 K, 656 K, 725 K, 757 K, and 784 K sequentially. We observed that each of the DB pairs occupied on a single dimer site, so we confirmed that the desorption mechanism of monohydride on Ge/Si(100)-2x1 also consisted of a pairing model in which a paired set of hydrogen atoms desorbed from a single dimer unit (section 1.4.1). At higher annealing temperature, many DB pairs formed zigzag chains as pointed by a white arrow in Fig. 3.1 (f).
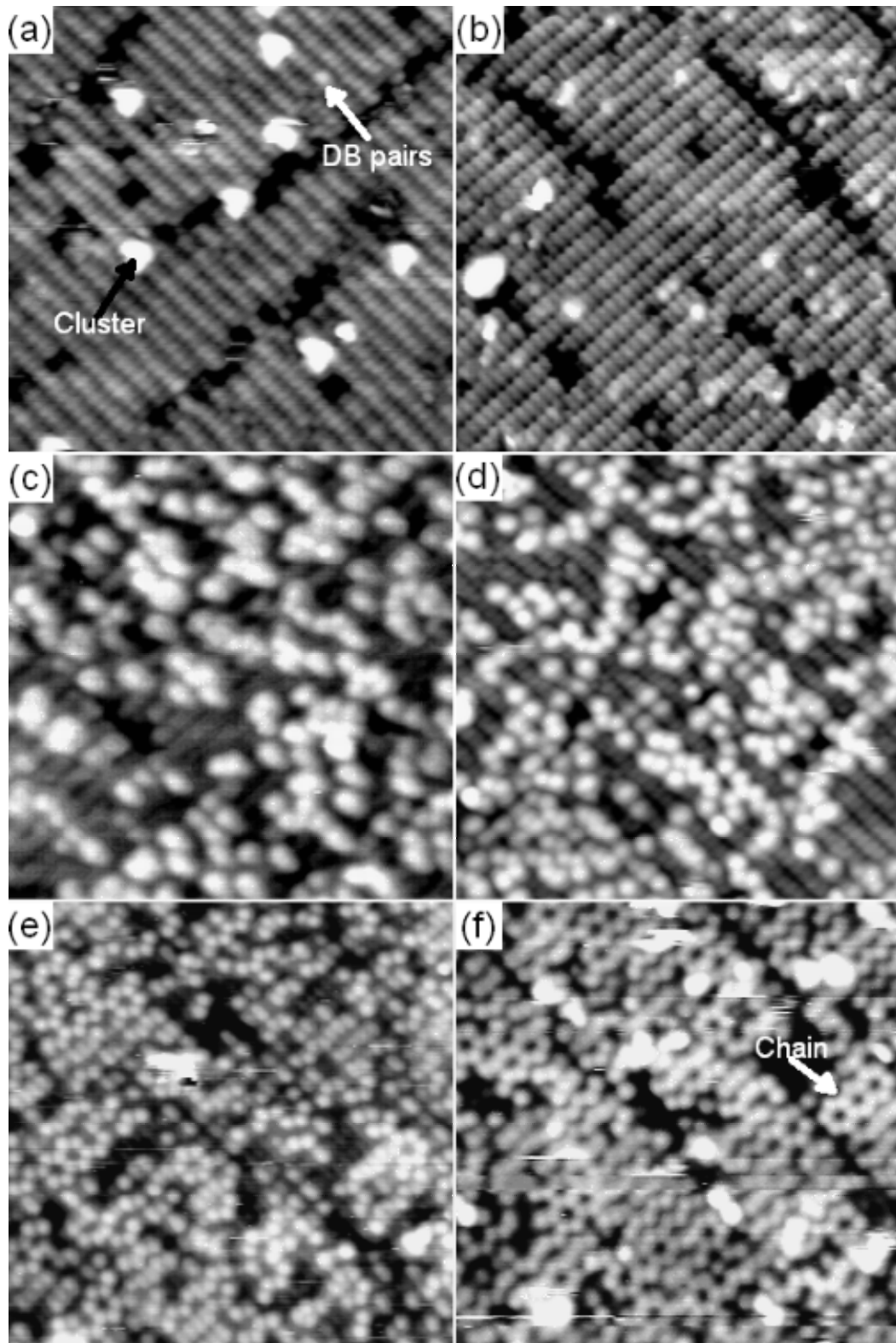
Fig. 3.1. The real-space STM images of the 0.4 ML Ge/Si(100)-2x1:H surface after annealing 1 min at (a) 0 K, (b) 592 K, (c) 656 K, (d)725 K, (e) 757 K, and (f) 784 K. The images are of size 150A x 150A. The sample bias is -2 volt.

Hirayama *et al.* indicated that these zigzag chains in STM images were produced by the asymmetry buckled dimer [20], as in Fig.3.2. The Ge-Si dimer was considered as a Ge-up/Si-down asymmetric structure because it was 0.55 eV more energetically favorable than the Ge-Si symmetric dimer.
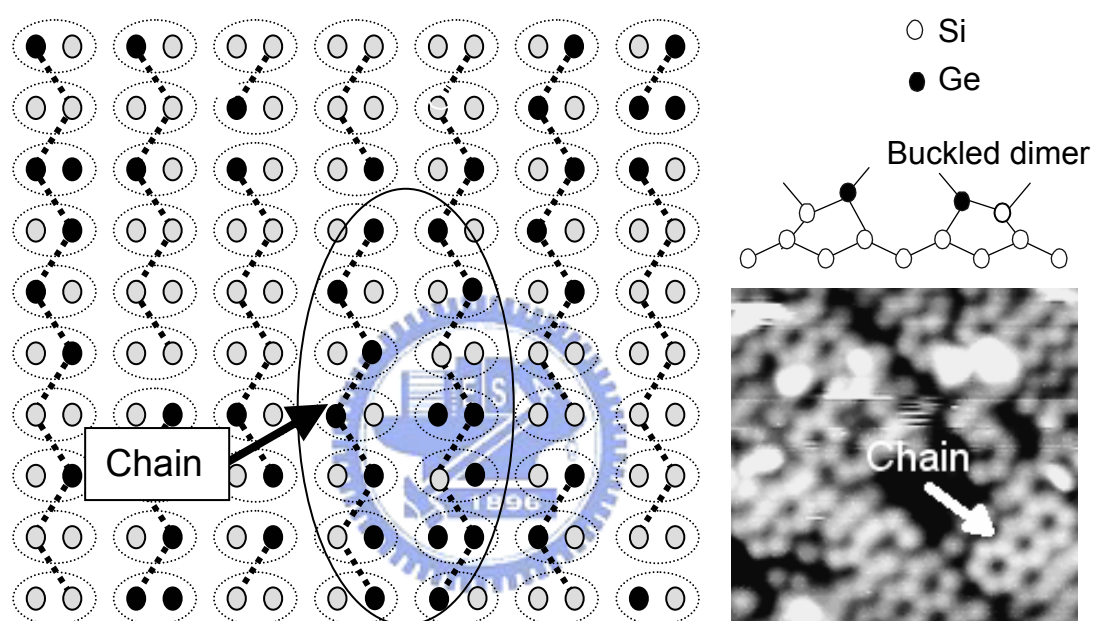

Fig. 3.2. The chain structure is formed by the asymmetry dimer structure. In the buckled dimer, Ge atoms are usually higher than Si atoms.

We also noticed that the amount of DB pairs apparently increased with the raising of annealing temperature obviously, and we could count the total sites of DB pairs in order to obtain the coverage of H_2 thermal desorption as shown in the next section.

3.1.2 The Number of DB Pairs Counted from STM Images

The H_2 desorption on the 0.4 ML Ge/Si(100)-2x1:H surface was observed by STM at various annealing temperatures between 530 K and 784 K. The DB pairs, *i.e.* bright sites in the STM images, were directly counted for analysis. The coverage of DB pairs with different annealing temperatures could be calculated individually. Taking Fig. 3.2 (d) for example, there are calculated totally 1059 DB pairs and 3542 dimers. Thus the coverage of DB pairs was 1059 / 3542 = 0.30 ML. The coverage of DB pairs vs. various annealing temperature were plotted in Fig. 3.3. It was obvious that the coverage increased with the annealing temperature. This result indicated that the H_2 desorption rate become faster at the higher temperature.

Hydrogen molecules could desorb from three possible dimer types (Ge-Ge, Ge-Si and Si-Si dimers). Although the STM images can directly "see" the Ge/Si surface atom by atom after H_2 desorption, which atoms (Ge or Si) below the DB pairs were still indistinguishable. In the following section, we will show that core-level photoemission which could provide us further information.
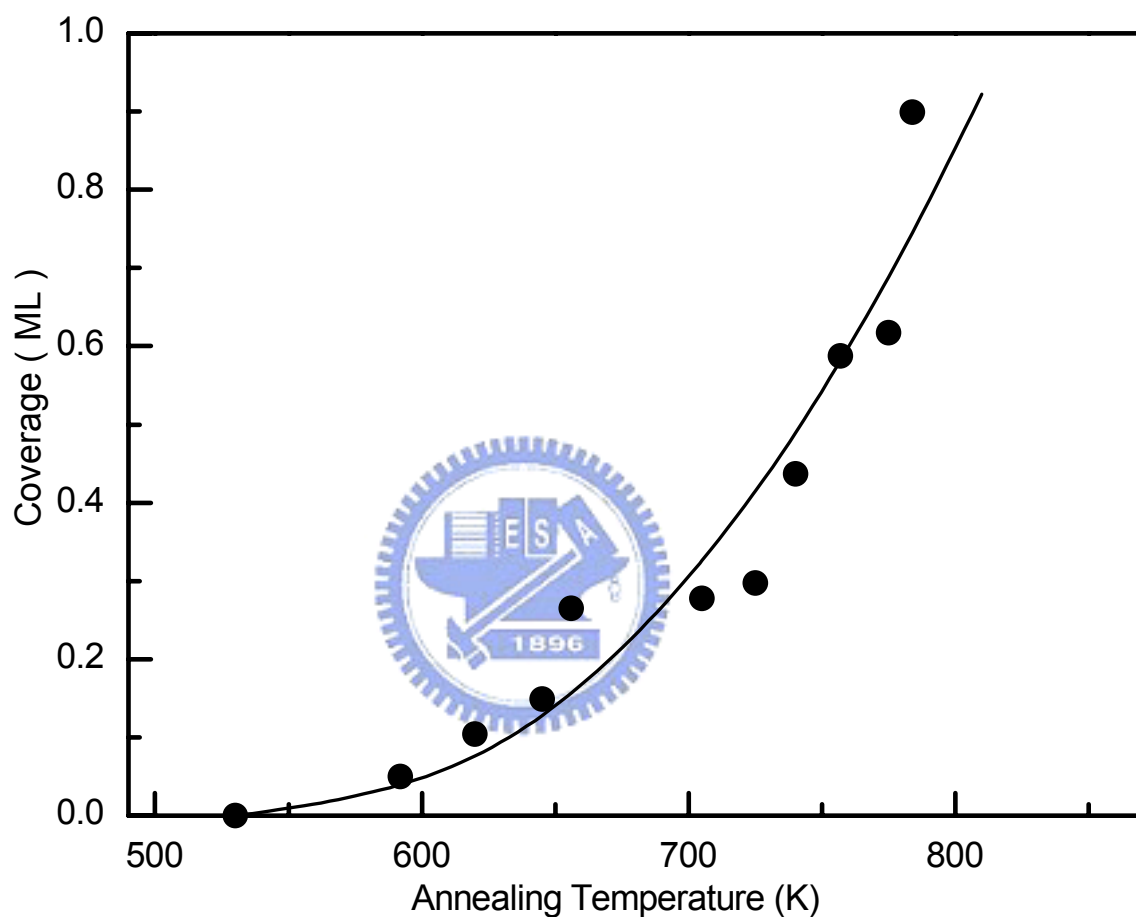
Fig. 3.3. The coverage of DB pairs was calculated by directly counting of the desorption sites at various annealing temperatures between 530 K and 784 K. The coverage of the DB pairs increases with the annealing temperature.

3.2   Photoemission Results and Analysis

In the core-level photoemission experiment, chlorine is exposed on the Ge/Si(100)-2x1:H surface after H_2 thermal desorption. The present Cl atoms can almost terminate all the DB pairs, as in Fig. 3.4, so the amount of Cl atoms will equate the number of dangling bonds. There is a dramatic energy shift in the photoemission spectra of the chlorine-terminated Ge/Si surface. This result makes it possible to analysis the proportion of chemical composition on the Ge/Si surface by the Si $2p$, Ge $3d$ and Cl $2p$ core level spectra. In this section, we will show both core level spectra in the Cl-terminated 0.4- and 0.8-ML Ge/Si(100)-2x1:H surfaces. Therefore, the amounts of H_2 desorption from Ge-Ge or Ge-Si or Si-Si dimers can be possibly deduced by the analysis of Si $2p$, Ge $3d$ and Cl $2p$ core level spectra.
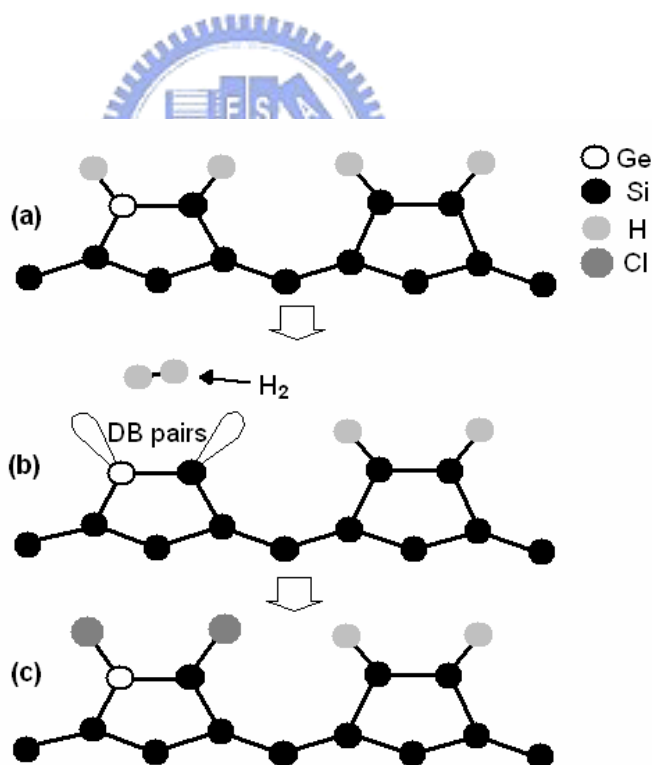

Fig. 3.4 The initial profile of the Ge/Si(100)-2x1:H surface shows in (a), and the same surface with the H_2 desorption and the Cl-terminated processes show in (b) and (c). The addition of Cl atoms will terminate the DB pairs.

This experiment was established on two hypotheses. The first hypothesis is that the impinging chlorine molecules would not react with the hydrogen atoms on the monohydride dimers. By exposing atomic hydrogen on the the Cl-saturated Si(111)-7x7 surface at RT, Iimori *et al.* observed that the hydrogen atoms extracted chlorine atoms from the chloride surface and formed HCl [21-22]. The simple energy gain is 83 kcal/mole after the reaction $SiCl + 2H \rightarrow SiH + HCl$. They also tried to observe another possible reaction, that is, molecular chlorine-induced extraction of hydrogen atoms on the H-saturated Si(111) surface. Their photoemission results showed no change in intensity either of Si2*p* core-level spectra or of the valence-band within experimental accuracy of 5%. This observation indicated that almost all hydrides on the surface do not react with chlorine gas. Therefore, it is expected that the impinging Cl molecules would not react with the hydrogen atoms on the Cl-saturated Si(100)-2x1 surface at RT.

The second hypothesis is that the diffusion, which tends to drive the surface towards the thermodynamic equilibrium distribution, is not instantaneous. Vizoso *et al.* proposed a model for H_2 thermal desorption from 0.61-ML Ge/Si(100) surface and obtained that the diffusion constant $K_{diff} = 6$ s^{-1} and the desorption constants $K = 3, 147, 7187$ s^{-1} for the Si-Si, Si-Ge, and Ge-Ge dimers respectively [7]. The diffusion rate was much smaller than the desorption rates from Si-Ge and Ge-Ge dimers indicating that desorption is a diffusion limited process. These results confirmed the assumption that the diffusion is not instantaneous.

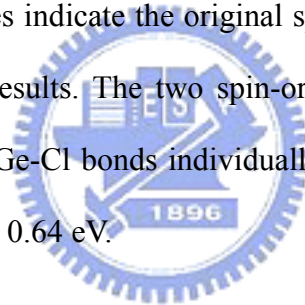### 3.2.1 H$_2$ Desorption from the 0.4-ML-Ge/Si(100) Surface

Cl 2*p* Spectra for the 0.4-ML-Ge/Si(100) Surface

In Fig. 3.5, the bottom spectrum shows the Cl 2*p* core-level spectrum on the Cl-saturated Si(100) surface. This spectrum was analyzed with one spin-orbit-split peak obviously, which was labeled as Cl$_s$, and it was caused by Cl-Si bonds. We regarded the binding energy of the bulk component in the Si 2*p* spectrum as the zero point energy, and all the spectra was adjusted with this condition. Therefore, the relative binding energy of Cl$_s$ spectrum is at about 99.5 eV.

The other spectra shown in Fig. 3.5 are the Cl 2*p* core-level spectra for the 0.4-ML-Ge/Si(100)-2x1:H surface which were saturated by Cl atoms after annealing at various temperatures as indicated. The widths of these spectra are broader than the widths of the spectrum for the Cl-saturated Si(100) surface. A fit to these spectra, it indicated that the Cl 2*p* spectra can be separated into two spin-orbit-split components, Cl$_s$ and Cl$_g$, which were caused by Cl-Si and Cl-Ge bonds individually. The spectra peak of Cl$_s$ term always stays at the same position, 99.56 eVrelative to the zero binding energy, and which of Cl$_g$ term lies in a lower relative binding energy. The difference in binding energy between Cl-Si and Cl-Ge is 0.64 eV and it is sufficient to identify the similar electron structure of Si and Ge.

The total intensity (total area below the Cl 2*p* spectrum) of Cl-saturated-Si(100) ssurface, is regarded as the coverage 1 ML. Therefore, coverage of the other spectra can be calculated by comparing the spectrum intensities with which at the Cl-saturated Si(100) surface.   The calculated coverage of each component in the Cl 2*p* core-level spectrum is depicted in Fig. 3.6.

Fig. 3.5 Photoemission spectra of the Cl $2p$ core level for the Cl-terminated Ge/Si(100)-2x1:H surfaces with various annealing temperatures 690 K, 729 K, and 793 K respectively. The open circles indicate the original spectrum, and the solid lines below this spectrum show our fitting results. The two spin-orbit-split components, Cl_s and Cl_g, are derived from the Si-Cl and Ge-Cl bonds individually and the difference in binding energy between Cl_s and Cl_g keeps in 0.64 eV.

0.4ML Ge/Si(100)-2x1: H
Cl 2p Core; hν= 240 eV

Cl_s

expose Cl_2
after anneal

793 K

Cl_g

729 K

690 K

Clean Si + Cl

Photoemission Intensity (arb. units)

Relative Binding Energy (eV)

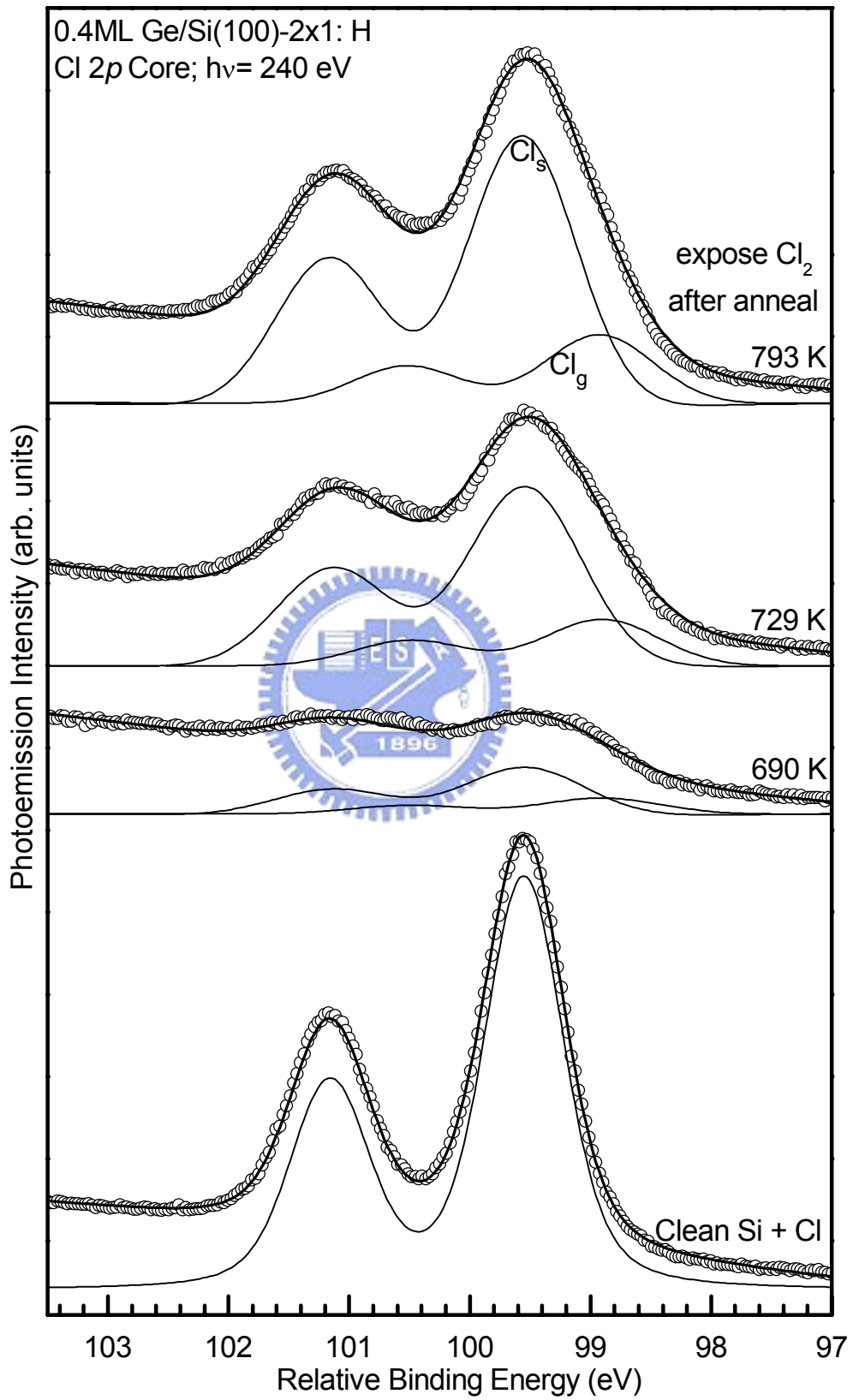103   102   101   100   99   98   97

Fig. 3.6 displays coverage procured from the direct DB pairs counting and the Cl $2p$ core-level-spectra analyses of the 0.4-ML-Ge/Si(100) surface. In Fig. 3.6, the "DB pairs" and "Cl 2p" components indicate the coverage of H_2 desorption which are obtained by two kinds of techniques, STM and core-level photoemission. Although the data is not fit perfectly, it is just regarded as a contrast with these two techniques. By the proportions between Cl_s and Cl_g components in Fig. 3.6, it is obvious that the coverage of Cl_s component is higher than Cl_g component and we will discuss this in the later section.

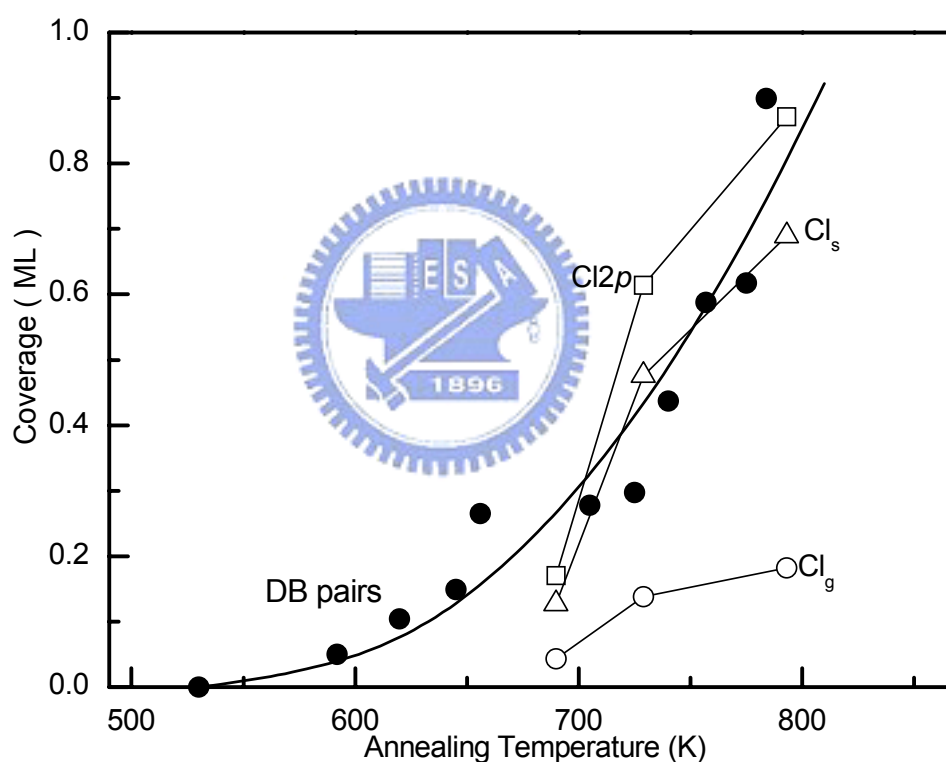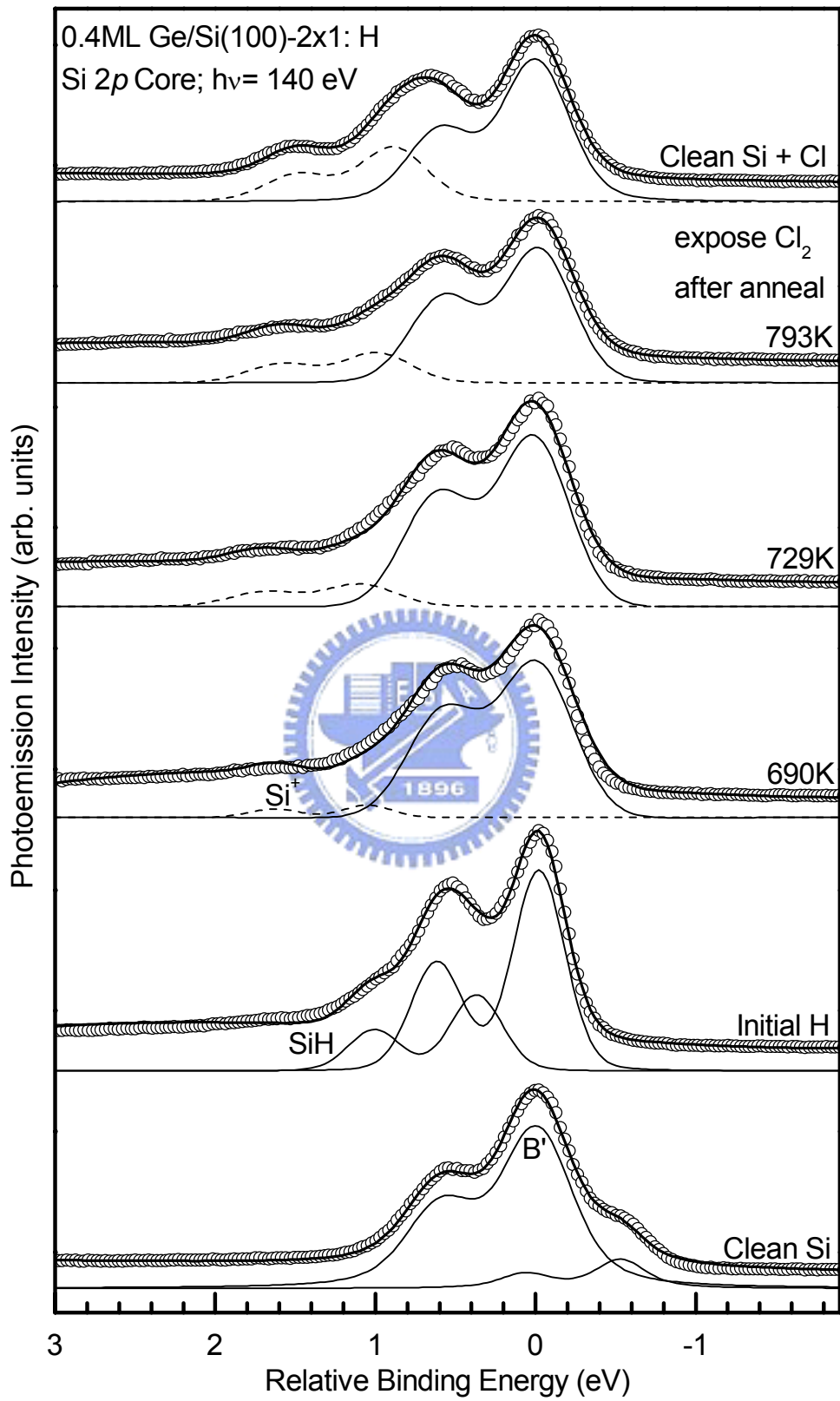Fig. 3.6 The 0.4-ML-Ge/Si(100)-2x1:H surface coverage procured from the STM DB pairs counting and the Cl $2p$ core level spectra analyses. The filled circles indicate the counting of STM DB pairs, the open squares indicate the coverage of the total Cl 2p core level spectra, and the open triangles and circles show the coverage of the two spin-orbit-split components, Cl_s and Cl_g, of Cl $2p$ core level spectra.

Si 2*p* Spectra for the 0.4-ML-Ge/Si(100) Surface

Figure 3.7 represents the Si 2*p* core-level spectra for the Cl-terminated 0.4-ML-Ge/Si(100)-2x1:H surface after annealing at various temperatures as indicated. The lowest spectrum of Fig.3.7 stands for the Si 2*p* spectrum on the clean Si(100) surface. This spectrum has two visible spin-orbital-split components which are labeled as B' and S. The B' component is caused by the terminated Si atoms at surface and the second-layer Si atoms, and the S component indicates the dangling bonds of Si atoms at surface. The difference in binding energy between B' and S is about 0.52 eV. The top of Fig.3.7 shows the Si 2p core-level spectrum on the Cl-saturated Si(100) surface, and it also has two spin-orbital-split component which label B' and Si^+. The Si^+ part is caused by Si-Cl bonds, and it has an energy shift 0.9 eV to the B' part. The other spectra are the Si 2*p* core-level spectra at the Cl-terminated 0.4-ML-Ge/Si(100)-2x1:H surfaces with different annealing temperatures as indicated. In Fig. 3.7, it is obvious that the intensities of Si^+ component rise with the increase of annealing temperature.

The ratio of the Si^+ intensity to the B' intensity for the Cl-saturated Si(100) spectrum is regarded as 1 ML coverage of the Si-Cl bonds on the surface, and this ratio is a constant which equals 0.38. The other coverage of the Cl-terminated 0.4-ML-Ge/Si(100)-2x1:H surface can be calculated by the normalized condition, and these result data are depicted into Fig. 3.8. The meaning of these data, the coverage of Si-Cl bonds, represents the DB pairs formed by H_2 desorption upon Si atoms of the dimers. The coverage of the Ge-Cl bonds will join in Fig. 3.8 later. The comparison of Si-Cl and Ge-Cl coverage express the amount of H_2 desorption from the Si atoms or Ge atoms individually.

Fig. 3.7 The Si 2*p* core level spectra represent for the Cl-terminated 0.4ML-Ge/Si(100)-2x1:H surface with various annealing temperature 690 K, 729 K, and 793 K respectively. The open circles indicate the original experiment spectrum; the solid and dash lines below the spectrum show our fitting results for this data. The dash line, which is labeled as Si^{+}, indicates the components of spectra for Si-Cl bonds.

0.4ML Ge/Si(100)-2x1: H
Si 2p Core; hν= 140 eV

Clean Si + Cl

expose Cl$_2$
after anneal

793K

729K

690K

Si$^+$

SiH

Initial H

B'

Clean Si

Photoemission Intensity (arb. units)
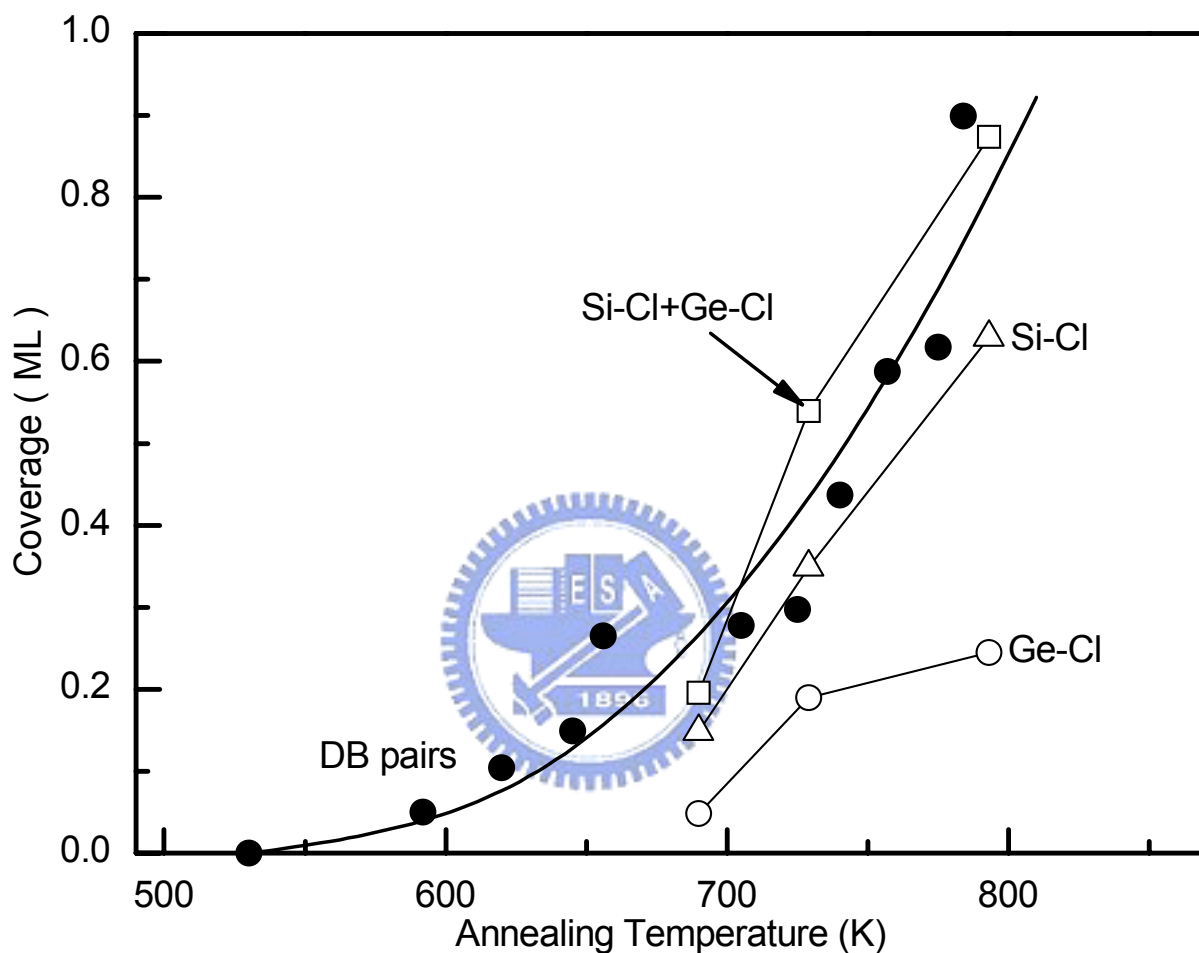
Relative Binding Energy (eV)

Fig. 3.8 The 0.4-ML-Ge/Si(100)-2x1:H surface coverage procured from the STM DB pairs counting and the Si/Ge core level spectra analysis. The filled circles indicated the counting of STM DB pairs directly, the open triangles indicate the coverage of the Si-Cl component of the Si 2p core level spectra, and the open circles show the coverage of the Ge-Cl component of the Ge 3d core level spectra respectively. The open squares represent the sum of the Si-Cl and Ge-Cl coverage.

Ge 3*d* Spectra for 0.4-ML-Ge/Si(100) Surface

The bottom spectrum in Fig. 3.10 represents the Ge 3*d* core-level spectra for the initial 0.4-ML-Ge/Si(100)-2x1 surface without H_2 adsorption and desorption. This spectrum has three obvious spin-orbital-split components and the structure of which shows in Fig. 3.9. The B component stands for the Ge bulk atoms; the S_u and S_d components indicate the dangling bonds with up-atom Ge and down-atom Ge of the asymmetry dimers at the surface respectively.
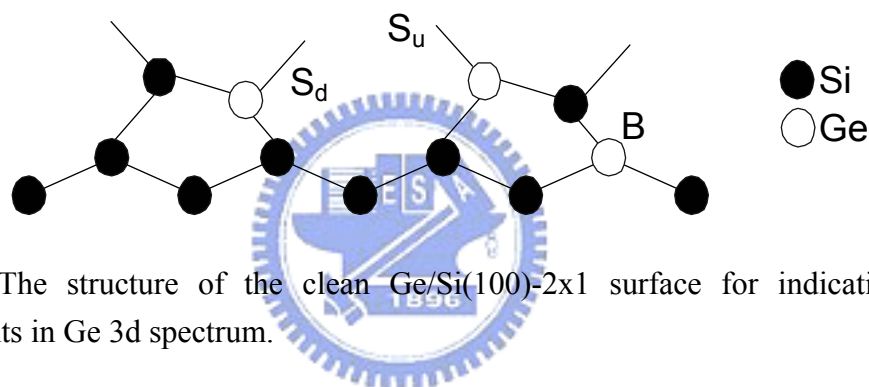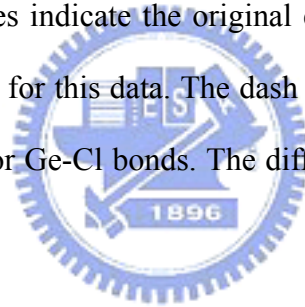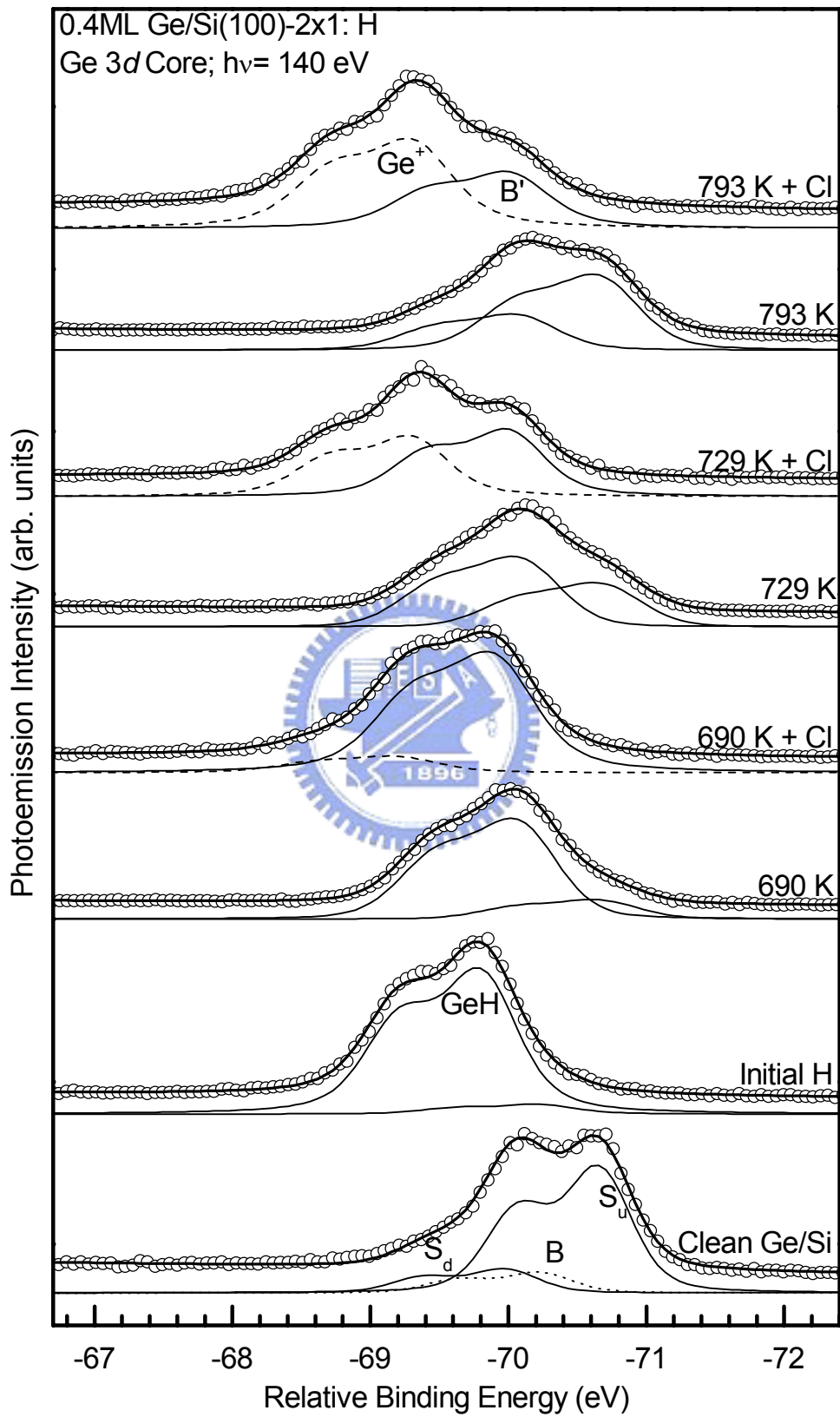

Fig. 3.9 The structure of the clean Ge/Si(100)-2x1 surface for indicating the three components in Ge 3d spectrum.

The second spectrum from the bottom of Fig. 3.10 stands for the H-saturated 0.4-ML-Ge/Si(100)-2x1 surface, and it merely consists of only one spin-orbital-split component which is caused by the Ge-H bonds. Some other spectra in Fig. 3.10 represent the Ge 3*d* core-level spectra for the 0.4-ML-Ge/Si(100)-2x1:H surface after annealing at various temperatures, and the others are the same surface after chlorine terminate on it as indicated. The Ge 3*d* spectra of the 0.4-ML- Ge/Si(100)-2x1:H surface after H_2 desorption has two visible spin-orbit-split components which label B' and S_u. The B' and S_u components are caused by the Ge bulk atoms and the dangling bonds upon Ge atoms respectively.

Fig. 3.10 Photoemission spectra for the Ge $3d$ core level represent for the Cl-terminated Ge/Si(100)-2x1:H surface with various annealing temperature 690 K,729 K, and 793 K respectively. The open circles indicate the original experiment spectra; the solid and dash lines show our fitting results for this data. The dash line, which is labeled as Ge^+, indicates the components of spectra for Ge-Cl bonds. The difference of binding energy between Ge^+ and B' keeps in 0.57 eV.

0.4ML Ge/Si(100)-2x1: H
Ge 3d Core; hν= 140 eV

Ge$^+$

B'

793 K + Cl

793 K

729 K + Cl

729 K

690 K + Cl

690 K

GeH

Initial H

S$_u$

B

S$_d$

Clean Ge/Si

Photoemission Intensity (arb. units)

Relative Binding Energy (eV)

-67   -68   -69   -70   -71   -72

After chlorine terminate the DB pairs on the same surface (the 0.4-ML-Ge/Si(100)-2x1:H surface after H_2 desorption), the S_u component disappears and the Ge^+ component emerges. Therefore, we considered that the Ge^+ component was caused by the Ge-Cl bonds. The difference of binding energy between Ge^+ and B' is 0.57 eV. The total intensity of the Ge 3d spectrum (the total area below the spectrum) is regarded as 0.4 ML. Then the coverage of the Ge-Cl bonds can be calculated by the intensity of the Ge^+ component relative to the total intensity of the spectrum. This result data is depicted in Fig. 3.11.

Summary for STM and Photoemission in 0.4-ML-Ge/Si(100) Surface

We integrate previous STM DB pairs counting and core-level-photoemission spectra analyses of 0.4-ML-Ge/Si(100) into Fig. 3.11. The coverage of Cl 2p core-level spectra (the sum of Cl_s and Cl_g) is very close to the total coverage of Si-Cl and Ge-Cl components in Si 2p and Ge 3d core-level spectra. In Fig. 3.11, the coverage of Cl_s component is higher than Si-Cl component and the coverage of Cl_g component is lower than Ge-Cl component, so the ratio of Si-Cl to Ge-Cl is lager in Cl2p spectra than in Si 2p /Ge 3d spectra. First, the analysis in Cl 2p core level can obtain the ratio of the Cl_s component to the Cl_g component directly. Next, the fitting result for the Si 2p and Ge 3d spectra is enormously changed with the little change of parameters in our analysis. For these two reasons, the ratio of Si-Cl to Ge-Cl bonds in the Cl 2p core-level analyses are considered to be more correct than in the Si 2p/Ge 3d spectra analysis. Therefore, we would use the analyses of Cl 2p core-level spectra for the latter discussion with the 0.8-ML- Ge/Si(100)-2x1:H surface.
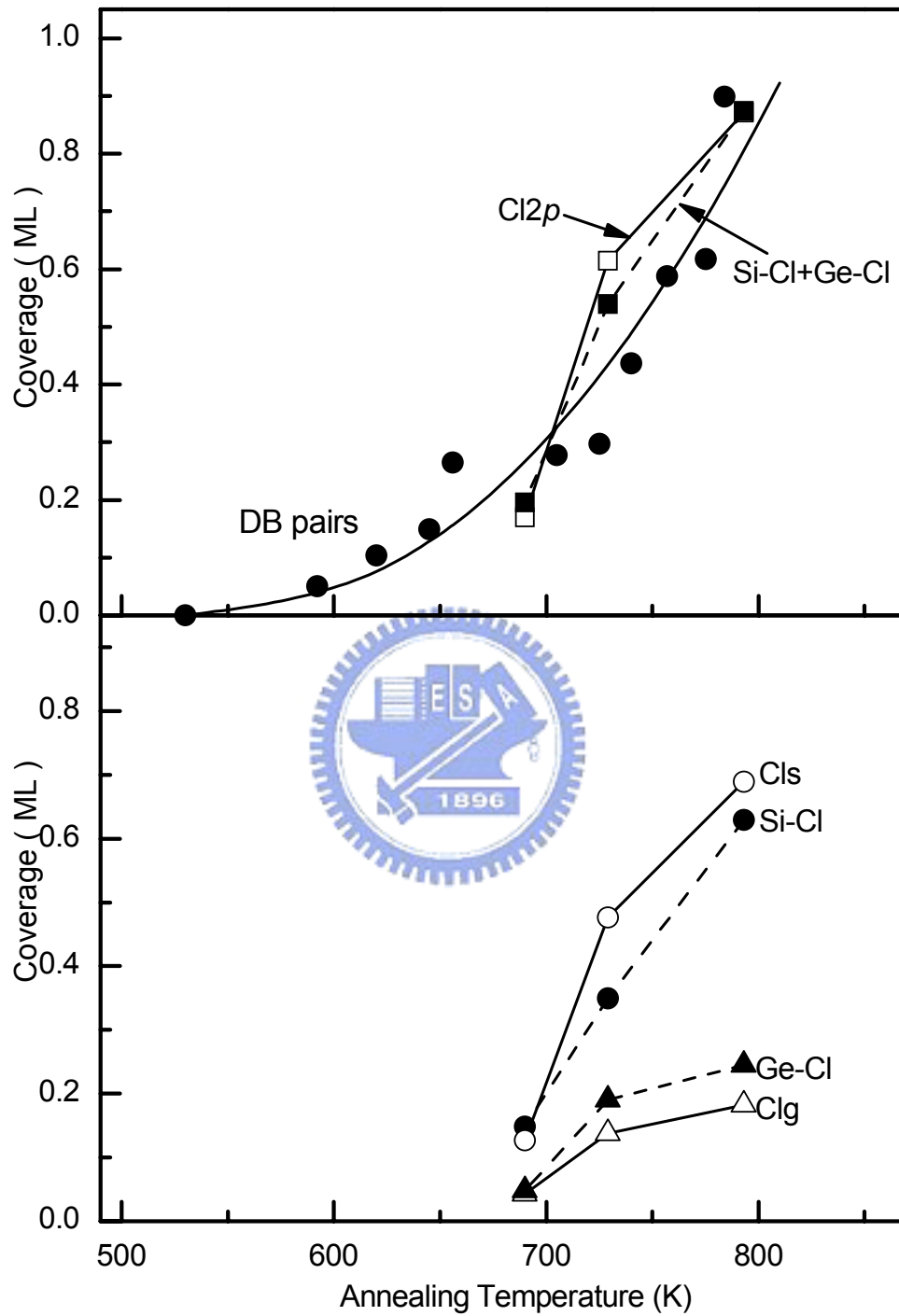
Fig. 3.11. The 0.4-ML-Ge/Si(100)-2x1:H surface coverage surveyed from three independent measurements: STM DB pairs counting, Cl2*p* core-level analysis, and Si2*p* /Ge*3d* core-level analysis.

3.2.2   H$_2$ Desorption from the 0.8-ML-Ge/Si(100) Surface

The analyses for the H$_2$ desorption from the 0.8 ML Ge/Si(100)-2x1:H surface are just the same with the previous analyses for the 0.4 ML Ge/Si(100)-2x1:H surface in section 3.2.1. Therefore, we directly show the Cl 2p and Si 2p /Ge 3d core-level spectra in Fig. 3.12 (a)-(c) and show the calculated coverage for these spectra in Fig. 3.12 (d).

The summary is as follows:

Fig. 3.12 (a) displays the Cl 2p core-level spectra for the Cl-terminated 0.8-ML-Ge/Si(100)-2x1:H surfaces after annealing at 633 K, 715 K, and 769 K respectively. We noticed that the spectrum with annealing temperature 769 K was the same as the spectrum for the clean 0.8-ML-Ge/Si(100)-2x1 surface (without H adsorption) which was only saturated by Cl atoms. This result was considered that the hydrogen molecules were entirely desorbed from the 0.8-ML-Ge/Si(100)-2x1:H surface at annealing temperature 769 K. Therefore, the intensity of this spectrum with annealing temperature 769 K was regarded as 1 ML and coverages of the other spectra in Fig. 3.12 (a) were able to be calculated by comparing with this intensity.

Fig. 3.12 (b) displays the Si 2p spectra for the Cl-terminated 0.8-ML-Ge/Si(100)-2x1:H surfaces.   Because the ratio of the Si$^+$ intensity to the B' intensity for the Cl-saturated Si(100) spectrum is regarded as 1 ML coverage of the Si-Cl bonds on the surface, and it is a constant 0.38.   Therefore, we can calculate all coverage of the Si$^+$ component in Fig. 3.12 (b) which indicates the coverage of the Si-Cl bonds on the surface.

Fig. 3.12 (c) displays the Ge 3d spectra for the Cl-terminated 0.8-ML-Ge/Si(100)-2x1:H surfaces. The total intensity of the Ge 3d spectrum (the total area below the spectrum) is regarded as 0.8 ML. Then the coverage of the Ge-Cl bonds can be

calculated by the intensity of the Ge$^+$ component relative to the total intensity of the spectrum.

The results of correlational analysis of Fig. 3.12 (a)-(c) are collected in Fig. 3.12 (d). In contrast with the DB pairs counted on the 0.4-ML-Ge/Si(100) surface in Fig. 3.12 (d), the calculated coverage of the spectra for the 0.8-ML-Ge/Si(100) surface, Cl2p and Si-Cl+Ge-Cl components, were the higher in the same temperature. This indicates that the H$_2$ desorption rate is faster on the 0.8-ML-Ge/Si(100) surface than in the 0.4-ML-Ge/Si(100) surface.

Although the coverage of Cl2p and Si-Cl+Ge-Cl in Fig. 3.12 (d) is very close to each other, the proportion of their composition is such different. We should determine one of the Cl2p and Si-Cl+Ge-Cl spectra to join the further discussion. For the two reasons that the analysis in Cl 2p core level can obtain the ratio of the Cl$_s$ component to the Cl$_g$ component directly, and the fitting result for the Si 2p and Ge 3d spectra is enormously changed with the little change of parameters in our analysis, the ratio of Si-Cl to Ge-Cl bonds in the Cl 2p core-level analyses are considered to be more correct than which in the Si 2p/Ge 3d spectra analysis. Therefore, we chose the Cl 2p spectra for the discussion in the next section.
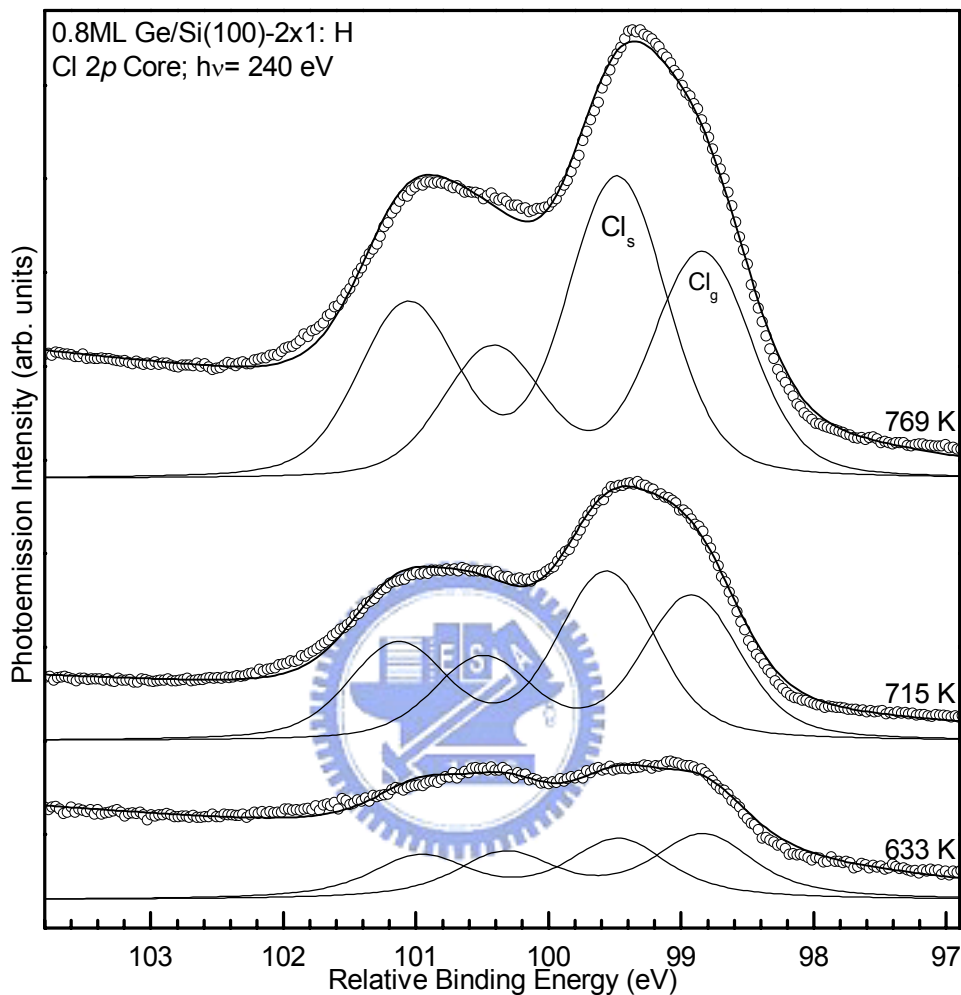
Fig. 3.12 (a). Photoemission spectra of the Cl $2p$ core level for the Cl-terminated Ge/Si(100)-2x1:H surfaces with various annealing temperatures 633 K, 715 K, and 769 K respectively. The open circles indicate the original experiment spectrum, and the solid lines below this spectrum show our fitting results. These two spin-orbit-split components, Cl_s and Cl_g, are derived from the Si-Cl and Ge-Cl bonds individually, and the difference in binding energy between Cl_s and Cl_g keeps in 0.64 eV.
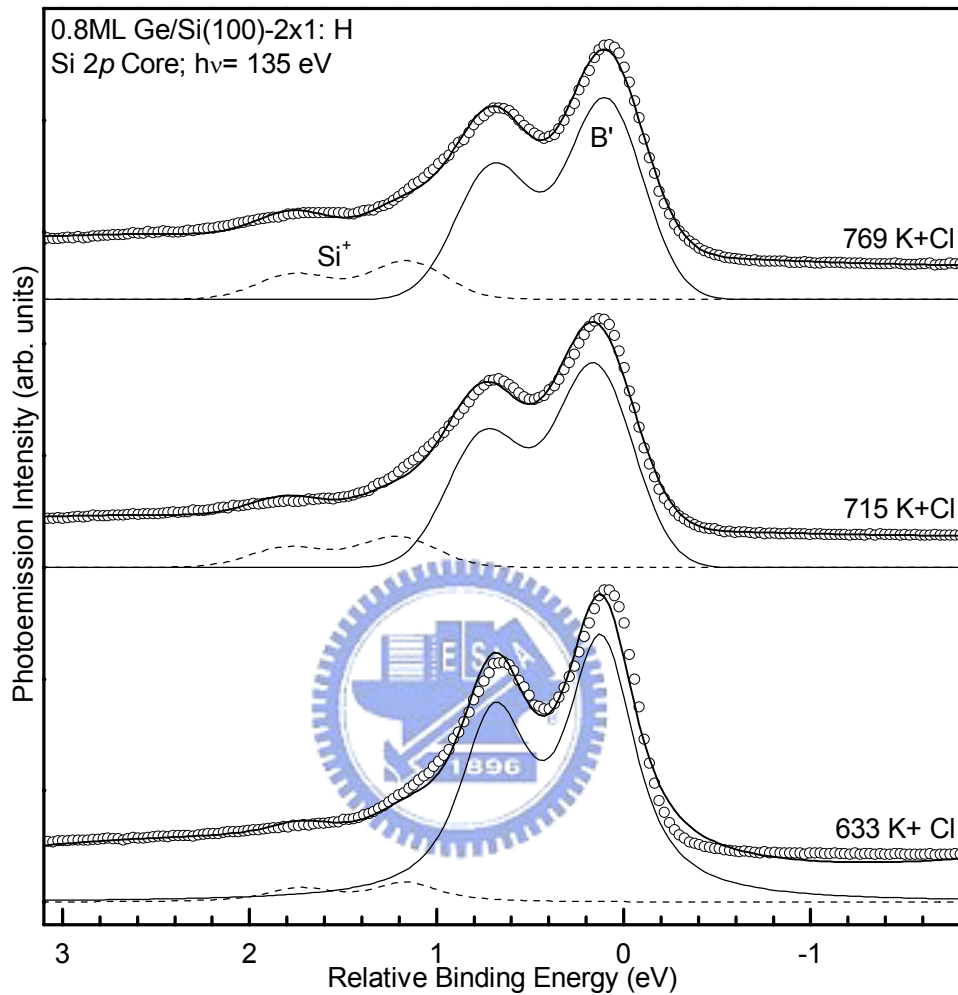
Fig. 3.12 (b). The Si 2*p* core level spectra represent for the Cl-terminated Ge/Si(100)-2x1:H surface with various annealing temperature 633 K, 715 K, and 769 K respectively. The open circles indicate the original experiment spectrum; the solid and dash lines below the spectrum show our fitting results for this data. The dash line, which is labeled as Si$^+$, indicates the components of spectra for Si-Cl bonds and the difference in binding energy between Si$^+$ and B' keeps in 0.9 eV.
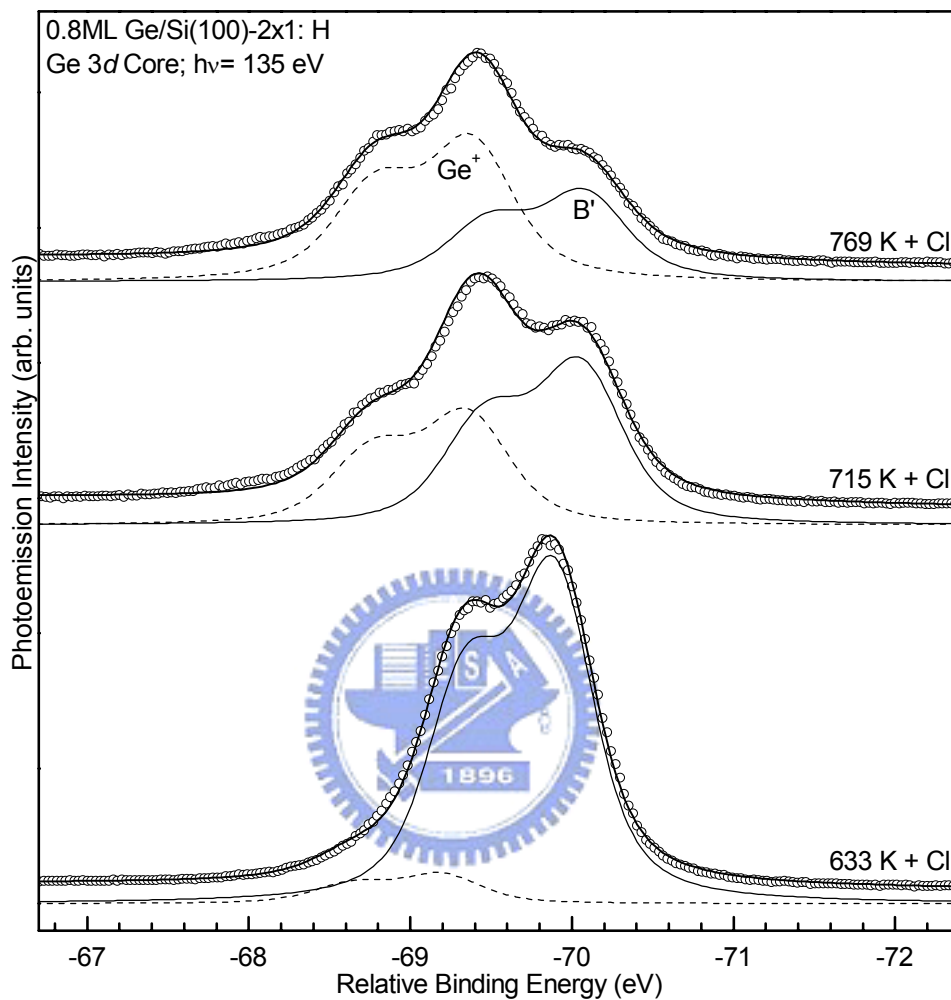
Fig. 3.12 (c) Photoemission spectra for the Ge $3d$ core level represent for the Cl-terminated Ge/Si(100)-2x1:H surface with various annealing temperature 633 K, 715 K, and 769 K respectively. The open circles indicate the original experiment spectra; the solid and dash lines show our fitting results for this data. The dash line, which is labeled as Ge^+, indicates the components of spectra for Ge-Cl bonds. The difference of binding energy between Ge^+ and B' keeps in 0.57 eV.
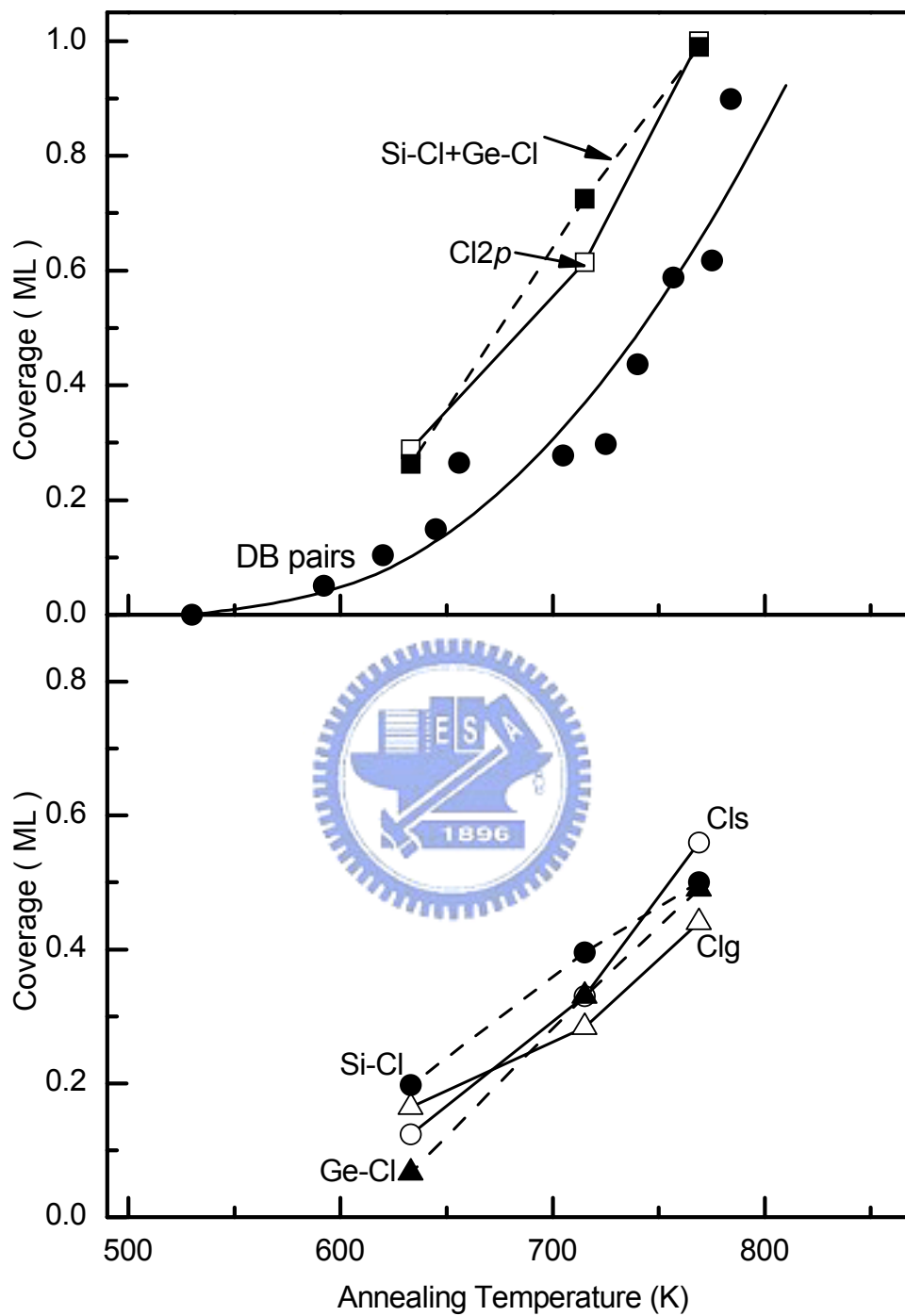
Fig. 3.12 (d). The 0.8-ML-Ge/Si(100)-2x1:H surface coverage surveyed from Cl2p and Si

2p /Ge 3d core-level analysis. The DB pairs indicates the coverage of H$_2$ desorption in the

0.4-ML-Ge/Si(100)-2x1:H surface previously.

3.3 H$_2$ Desorption from Various Kinds of Dimers on Ge/Si(100) Surface

After exposing Ge$_2$H$_6$ on the Si(100) substrate and annealing at 950 K, the surface consists of Ge-Ge, Ge-Si, and Si-Si intermixing Ge/Si(100)-2x1 surface. If we saturate the DBs with Cl atoms on the Ge/Si surface, we can distinguish Ge atoms from Si atoms on the surface from the STM images [6]. The Cl atoms bonded with Ge is brighter than that bonded with Si in STM images. By counting the amount of Ge atoms on the 0.4- and 0.8-ML-Ge/Si(100)-2x1:H surfaces from STM images, we got the result that there were approximately 0.33 ML Ge-Cl bonds on the 0.4-ML-Ge/Si(100) surface and 0.56 ML Ge-Cl bonds on the 0.8-ML-Ge/Si(100) surface [6]. We referred the reduction of Ge coverage on the surface to the reaction of Si/Ge place exchange.

Angot *et al.* suggested that the H$_2$ desorption from Ge-Ge, Ge-Si, and Si-Si dimers were at different temperatures 463 K, 623 K, and 743 K because the energy of Ge-H bonds is lower than the energy of Ge-H bonds[8]. The work of Vizoso *et al.* exhibited that the desorption rates of H from the Ge-Ge and Ge-Si dimers are much faster than from the Si-Si dimer. Therefore in our initial thought, hydrogen molecules would desorb from the Ge-Ge, Ge-Si, and Si-Si dimers in sequence. In this scenario, we can calculate the dimer components of the H$_2$ desorption at various annealing temperatures from 0.4- and 0.8-ML-Ge/Si(100) surface. This calculated result is shown in Fig. 3.13. It is obvious that the expected analysis is quite different to our experiment. The forecast of H$_2$ desorption at lower annealing temperature should be accomplished by the most Ge-Ge and Ge-Si dimers and a small amount of the Si-Si dimers. The ideal forecast is that the Cl-Ge component must be higher than the Cl-Si component, but the experiment displayed different result.
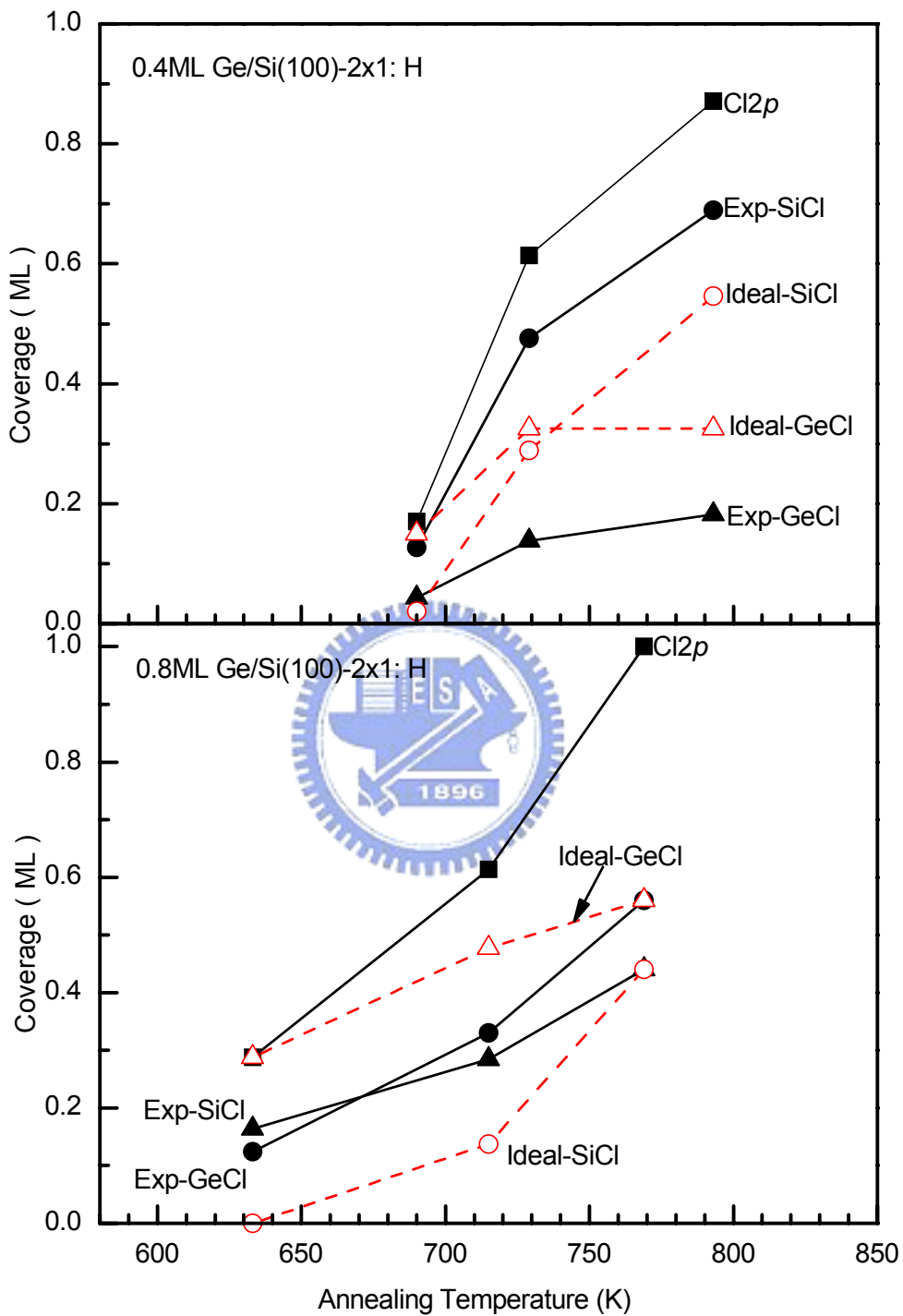
Fig. 3.13. The ideal forecast and experimental results for the H_2 desorption from 0.4- and 0.8-ML-Ge/Si(100) surface.

There are three possible reactions which could cause these experiment results. First, the impinging Cl_2 react with the H atoms on the surface. Second, the diffusions of H atoms occur on the surface. Third, the places of Ge/Si atoms exchange in the surface layers.

If the reaction between the impinging Cl_2 and the H atoms on the surface occur quickly, the Cl atoms will take the place of the H atoms greatly. In order to observed the influence of the impinging Cl_2 and the H atoms, the Cl_2 gas was used to exposed to the H-saturated Si(100) surface. Therefore, we obtained the photoemission spectra for this surface and showed it in the Fig. 3.14(a). The intensity of the Cl $2p$ spectrum for the H-saturated Si(100) surface after Cl exposing is less than 4 % of that for the Cl-saturated Si(100) surface. This indicates that the reaction of impinging Cl_2 with the H atoms on the surface is very slightly.

Vizoso *et al.* proposed a model for H_2 thermal desorption from 0.61-ML Ge/Si(100) surface and obtained that the diffusion constant $K_{diff} = 6$ s^{-1} and the desorption constants K = 3, 147, 7187 s^{-1} for the Si-Si, Si-Ge, and Ge-Ge dimers respectively [7]. The diffusion rate was much smaller than the desorption rates from Si-Ge and Ge-Ge dimers indicating that desorption is a diffusion limited process.

In the report of Angot *et al*. [11], they proposed that the Ge-Ge dimers on the Ge/Si surface would transform into the Ge-Si dimers during the H_2 desorption process above 200 ℃ (473 K). The energetic balance is very unfavorable to allow the Ge-Ge dimer with free surface dangling bonds to remain at the surface. The formation of the Ge-Si dimers had been considered as an energetically more favorable surface topology [23-24]. Therefore, we assumed that most Ge-Ge dimers transformed into Ge-Si dimers. According to this assumption, we calculated the the dimer components of the H_2 desorption at various annealing temperatures from 0.4- and 0.8-ML-Ge/Si(100) surface again and showed the modified result in Fig. 3.15.
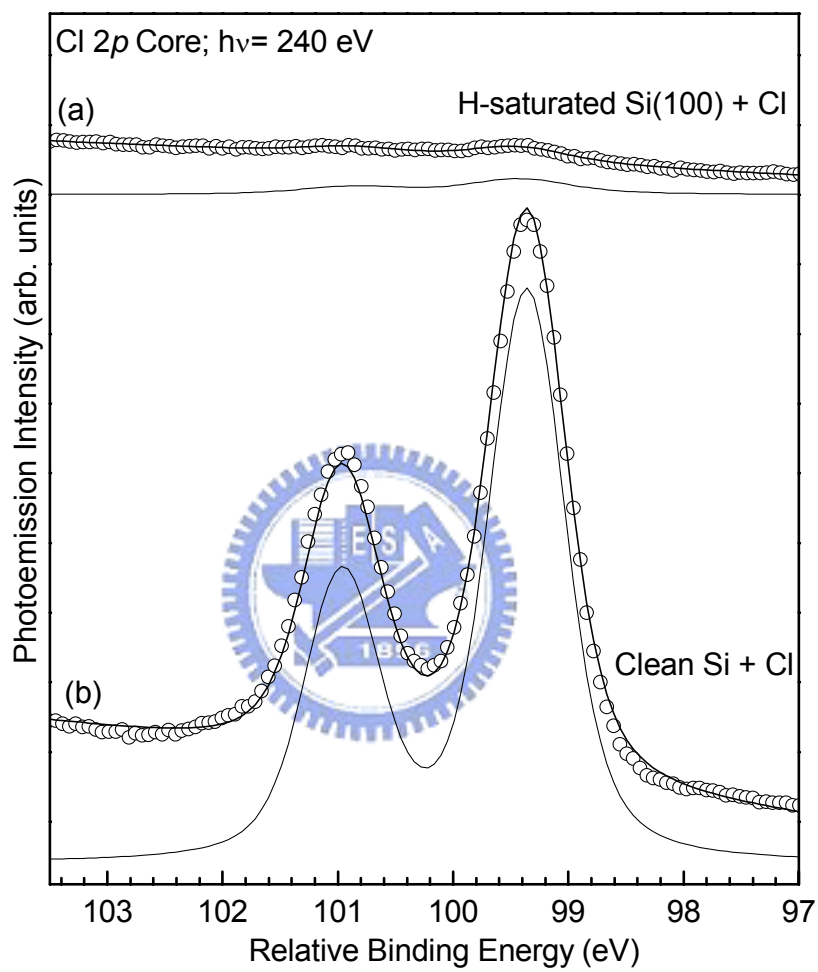
Fig. 3.14. (a) The Cl *2p* spectrum for the H-saturated Si(100) surface after Cl exposing. (b)

The Cl *2p* spectrum for the Cl-saturated Si(100) surface.

In Fig. 3.15, the result is excellent agreement with the coverage of Si-Cl and Ge-Cl components in the 0.8-ML-Ge/Si(100) surface. But it is obvious that the result is inconsistent with the coverage of Si-Cl and Ge-Cl components in the 0.4-ML-Ge/Si(100) surface. The ratio of Si-Cl component to Ge-Cl component in experimental result was higher than in the expected result. In the resent work of Kutana *et al.* (2003), they indicated that the H_2 desorption from Si(100) surface had proceed at the temperature 720 K obviously [15]. We proposed that the H_2 desorption from Si-Si dimer proceed above 720 K, as the dash line in Fig. 3.15. Therefore, the hydrogen molecules were desorbed from the Ge-Si and Si-Si dimes simultaneously at the desorption temperature above 720 K. This analysis confirmed that the replacement reaction of Ge/Si atoms occurred during H_2 desorption indeed.
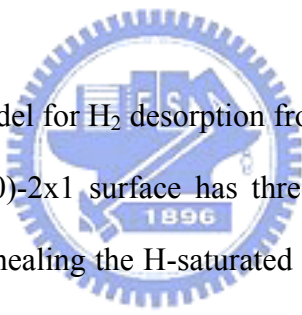
Figure 3.16 shows a model for H_2 desorption from the Ge/Si(100)-2x1 surface. (a) The initial H-saturated Ge/Si(100)-2x1 surface has three kinds of dimers Ge-Ge, Ge-Si, and Si-Si on its top layer. (b) Annealing the H-saturated Ge/Si surface below 650 K causes that the Ge atoms and Si atoms exchange their place making H-Ge-Ge-H transform into H-Ge-Si-H. (c) Hydrogen molecules start to desorb from the Ge-Si dimers at annealing temperature about 650 K. (d) Hydrogen molecules start to desorb from the Si-Si dimers at annealing temperature about 720 K.
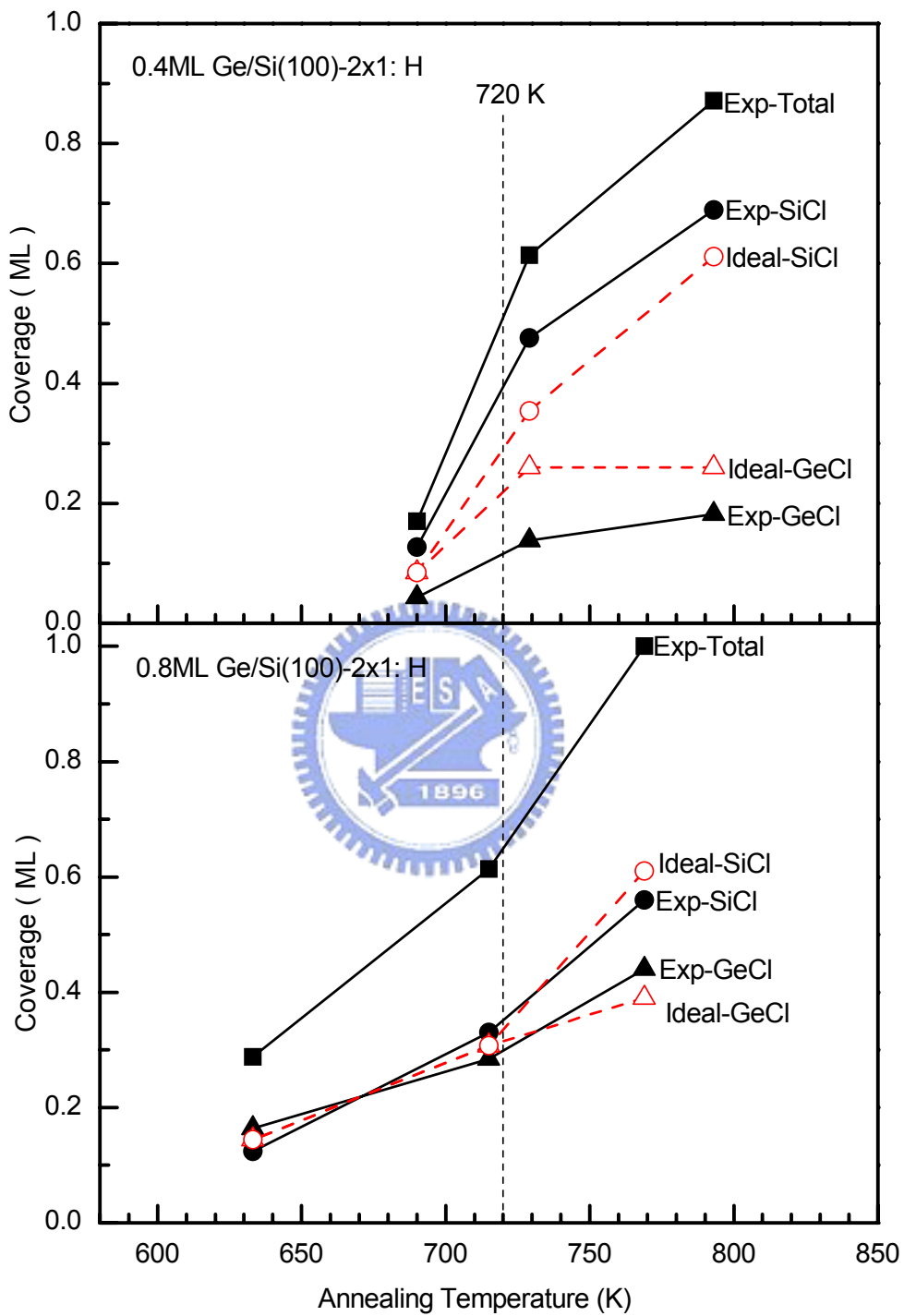
Fig. 3.15 The ideal forecast and experimental results for the H_2 desorption from 0.4- and 0.8-ML-Ge/Si(100) surface.
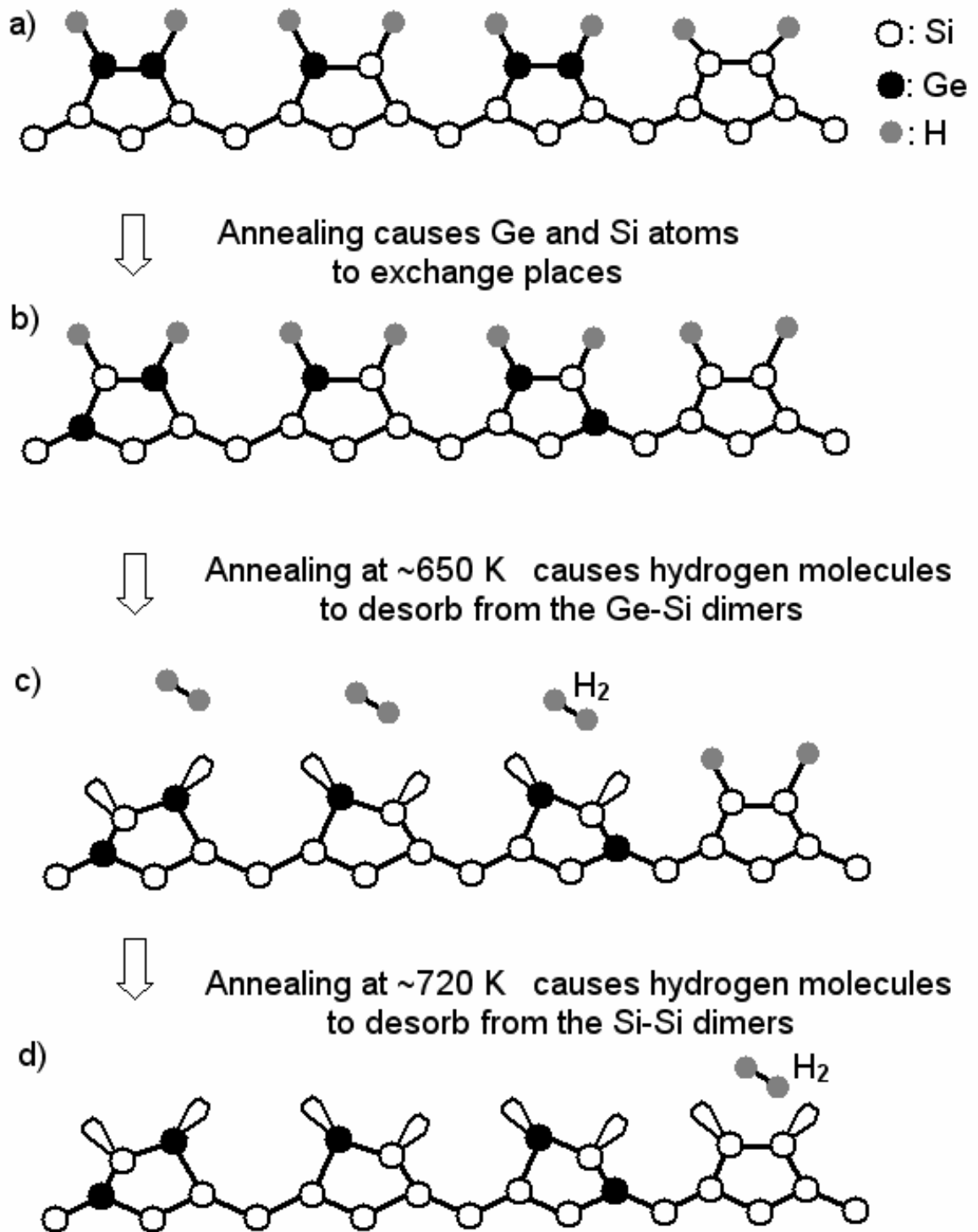
Fig. 3.16. A model for the H_2 desorption from the Ge/Si(100)-2x1 surface.

CHAPTER 4

CONCLUSIONS

The heterostructure of the SiGe alloy and Si(100) substrate has practical applications in optical and electronic devices. The hydrogen desorption is an important process controlling the growth rate of Ge_xSi_{1-x} in CVD. In addition, hydrogen is one of the simplest adsorbates to study adsorption, reaction, and desorption processes on the semiconductors and therefore often serve as model system. The purpose of this study was to gain more detailed understanding of the mechanism of the H_2 thermal desorption from the GeSi alloy.

Two complementary techniques, *i.e.* STM and core-level photoemission, are employed to probe the H-covered Ge/Si(100) surfaces and study the mechanism of the H_2 desorption from the Ge-Ge, Ge-Si, and Si-Si dimers in the top surface layer. The chlorine atoms were used to saturate the surface after partial H_2 desorption and to act as a marker in photoemission spectra. We started our experiment based on two hypotheses. The first hypothesis is that the impinging chlorine molecules would not react with the hydrogen atoms on the monohydride dimers. The second hypothesis is that the diffusion of surface hydrogen, which tends to drive the surface towards the thermodynamic equilibrium distribution, is not instantaneous.

Our conclusions are summarized in the following.

(1) The number of DB pairs, i.e. the amount of hydrogen desorption sites, from the 0.4-ML-Ge/Si(100) surface increase with the annealing temperature. Although the STM images can directly "see" the Ge/Si surface atom by atom after H_2 desorption, which atoms (Ge or Si) below the DB pairs were still indistinguishable.

(2) After exposing hydrogen onto the 0.4-ML- and 0.8-ML-Ge/Si(100) surfaces at about 600 K, the intensities of the GeH component (H atoms bonded with Ge atoms in the surface) in the Ge $3d$ core-level spectra were much larger than that of the bulk component. This result indicated that during H_2 adsorption most Ge atoms still stayed at the top layer of the surface and the replacement of Ge/Si atoms did not occur.

(3) After partial H_2 desorbing from the H-saturated Ge/Si(100) surface and Cl_2 passivation, the intensity of the Cl-Si component in Cl $2p$ core-level spectra was much higher than that of the Cl-Ge component. This indicated that the amount of H_2 desorbing from the Si atoms was larger than from the Ge atoms on the dimer structure.

Angot *et al.* measure the intensity variation of the stretching modes with annealing temperature for the Si(100), Ge(100), and 0.5-ML-Ge/Si(100) surfaces by high resolution electron energy loss spectroscopy (HREEL). They found that the H_2 desorption from Ge-Ge, Ge-Si, and Si-Si dimers were at different temperatures 463 K, 623 K, and 743 K. They attributed this result to the lower energy of Ge-H bonds than that of Si-H bonds [8]. If H_2 did desorb from this case, the hydrogen molecules would start to desorb from Ge-Ge dimers at a lower temperature, from Ge-Si dimers at a little higher temperature, and from Si-Si dimers at a higher temperature. Consequently, the intensity of the Cl-Ge component must be larger than that of the Cl-Si component in Cl $2p$ core-level spectra below 743 K. However, our experimental result was different from this ideal case.

The formation of the Ge-Si dimers had been considered as an energetically more favorable surface structure [23-24]. The recent reports suggested that the exchange of Ge and Si atoms would occur during the H_2 desorption from Ge/Si surface making the most

Ge-Ge dimers transform into the Ge-Si dimers. In addition, the bulk component became comparable with the Cl-Ge component in the Ge 3d core-level spectra. Therefore, the place-exchange reaction of the Ge/Si atoms on the surface was likely lead to these experimental results, as shown in Fig. 3.16.

References

[1] D. A. Neamen, *Semiconductor Physics & Devices*, 3rd ed. (McGraw-Hill, 2002).

[2] D. J. Paul, Adv. Mater. **11**, 191 (1999).

[3] J. P. Liu, D. D. Huang, J. P. Li, Y. X. Lin, D. Z. Sun, And M. Y. Kong, J. Appl. Phys. **85**,6920 (1999).

[4] B. M. H. Ning and J. E. Crowel, Appl. Phys. Lett. **60**, 2914 (1992).

[5] K.-H. Huang, T.-S. Ku, and D.-S. Lin, Phys. Rev. B **56**, 4878 (1997).

[6] D.-S. Lin, J.-L. Wu, S.-Y. Pan, and T.-C. Chiang, Phys. Rev. Lett. **90**, 046102 (2003).

[7] J. Vizoso, F. Martín, J. Suñé, and M. Nafría, J. Vac. Sci. Technol. A **15**, 2693 (1977).

[8] T. Angot and P. Louis, Phys. Rev. B **60**, 5938 (1999).

[9] E. S. Tok, S. W. Ong, and H. C. Kang, J. Chem. Phys. **120**, 5424 (2004).

[10] E. Rudkevich, Feng Liu, D. E. Savage, T. F. Kuech, L. McCaughan, and M. G. Lagally, Phys. Rev. Lett. **81**, 3467 (1998).

[11] T. Angot and P. Louis, Phys. Rev. B **61**, 7293 (2000).

[12] M. M. Bülbül, M. Çakmak, G. P. Srivastava, and K. Çolakoğlu, Phys. Rev. B **64**, 155318 (2001).

[13] J. J. Boland, Phys. Rev. Lett. **65**, 3325 (1990).

[14] A. Kubo, Y. Ishii, and M. Kitajima, J. Chem. Phys. **117**,11336 (2002).

[15] A. Kutana, B. Makarenko, and J. W. Rabalais, J. Chem. Phys. **119**, 11906 (2002).

[16] D.-S. Lin, S.-Y. Pan, and M.-W. Wu, Phys. Rev. B **64**, 233302 (2001).

[17] M.-W. Wu, S.-Y. Pan, W.-H. Hung, and D.-S. Lin, Surf. Sci. **507-510**, 295 (2002).

[18] J. J. Boland, Phys. Rev. Lett. **67**, 1539 (1991).

[19] M. P. D'Evelyn, S. M. Cohen, E. Rouchouze, and Y. L. Yang, J. Chem. Phys. **98**, 3560 (1993).

[20] H. Hirayama, H. Mizuno, R. Yoshida, Phys. Rev. B **66**, 165428 (2002).

[21] T. Iimori, K. Hattori, K. Shudo, F. Komori, Surf. Sci. **437**, 86 (1999).

[22] K. Hattori, K. Shudo, M. Ueta, T. Iimori, Surf. Sci. **402-404**, 170 (1998).

[23] S. J. Jenkins and G. P. Srivastava, Surf. Sci. **377-379**, 887 (1996).

[24] R. H. Miwa, Surf. Sci. **418**, 55 (1998).